THE JOURNAL OF BIOLOGICAL CHEMISTRY VOL. 287, NO. 51, pp. 43137–43155, December 14, 2012

Bromodomain-containing Protein 4 (BRD4) Regulates RNA Polymerase II Serine 2 Phosphorylation in Human CD4+ T Cells*[S]

Received for publication, August 23, 2012, and in revised form, October 7, 2012 Published, JBC Papers in Press, October 19, 2012, DOI 10.1074/jbc.M112.413047

Weishi Zhang[‡1], Celine Prakash[‡1], Calvin Sum[‡1], Yue Gong[‡], Yinghui Li[‡§], Jeffrey J. T. Kwok[‡], Nina Thiessen[¶], Sven Pettersson[§], Steven J. M. Jones[¶], Stefan Knapp[‖], Henry Yang[**], and Keh-Chuang Chin[‡§§2]

*From the [‡]Laboratory of Gene Regulation and Inflammation, SIgN (Singapore Immunology Network), A*STAR (Agency for Science, Technology and Research), Biopolis, Immunos 04-00, 8A Biomedical Grove, Singapore 138648, the [§]Department of Microbiology, Cell and Tumor Biology, Karolinska Institutet, Stockholm 171 77, Sweden, the [¶]Bioinformatics Laboratory, Canada's Michael Smith Genome Sciences Centre, Vancouver, British Columbia V5Z 1L3, Canada, the [‖]University of Oxford, Structural Genomics Consortium, Old Road Campus Research Building, Roosevelt Drive, Headington, Oxford OX3 7DQ, United Kingdom, the [**]Bioinformatics Group, Singapore Immunology Network (SIgN), Agency for Science, Technology and Research (A*STAR), 8A Biomedical Grove, 04-06 Immunos, Singapore 138648, and the [§§]Department of Physiology, Yong Loo Lin School of Medicine, National University of Singapore, Singapore 117573*

Background: BRD4 interacts with P-TEFb, which regulates Pol II elongation.
Results: Disruption of BRD4 binding by JQ1 resulted in reduced Pol II Ser-2 in CD4+ T cells.
Conclusion: BRD4 affects Pol II Ser-2 phosphorylation at a subset of lineage-specific active genes in primary human CD4+ T cells.
Significance: BRD4 binding may represent a means of identifying active promoters and lineage-specific enhancer elements.

Transcriptional elongation by RNA polymerase II (Pol II) is regulated by positive transcription elongation factor b (P-TEFb) in association with bromodomain-containing protein 4 (BRD4). We used genome-wide chromatin immunoprecipitation sequencing in primary human CD4+ T cells to reveal that BRD4 co-localizes with Ser-2-phosphorylated Pol II (Pol II Ser-2) at both enhancers and promoters of active genes. Disruption of bromodomain-histone acetylation interactions by JQ1, a small-molecule bromodomain inhibitor, resulted in decreased BRD4 binding, reduced Pol II Ser-2, and reduced expression of lineage-specific genes in primary human CD4+ T cells. A large number of JQ1-disrupted BRD4 binding regions exhibited diacetylated H4 (lysine 5 and -8) and H3K27 acetylation (H3K27ac), which correlated with the presence of histone acetyltransferases and deacetylases. Genes associated with BRD4/H3K27ac co-occupancy exhibited significantly higher activity than those associated with H3K27ac or BRD4 binding alone. Comparison of BRD4 binding in T cells and in human embryonic stem cells revealed that enhancer BRD4 binding sites were predominantly lineage-specific. Our findings suggest that BRD4-driven Pol II phosphorylation at serine 2 plays an important role in regulating lineage-specific gene transcription in human CD4+ T cells.

Regulation of gene transcription occurs at both initiation and elongation phases (1, 2). Phosphorylation of serine 5 (Ser-5) in the C-terminal domain of RNA polymerase II (Pol II)[3] is associated with initiation (3, 4), whereas Pol II phosphorylation at Ser-2 is mediated by positive transcription elongation factor b (P-TEFb) and is associated with elongation (5). P-TEFb association with Pol II depends on tethering factors such as transcription factor c-Myc, which is recruited to one-third of all active genes in mouse embryonic stem cells (2).

Bromodomain-containing protein 4 (BRD4) is a nuclear protein that contains two bromodomains (BD1 and BD2) (6). BRD4 interacts with acetylated lysines, but the exact combination of modified histone tails required to recruit BRD4 to target genes is unknown. For example, *in vitro* assays indicate that BRD4 binding can be supported by diacetylated histone 3 (H3) at lysines K9/14, and by di-acetylated histone 4 (H4) at lysines K5/12, as well as by tetra-acetylated H4K5/8/12/16 peptides (7). In contrast, *in vivo* studies have identified acetylation at histone H4K5/8/12 (8) and H3K9acS10ph/H4K16ac (9) as BRD4 recognition sites. BRD4 has also been implicated in the recruitment of P-TEFb and transcription elongation (8, 10), but the

* This work was supported by SIgN (A*STAR, Singapore).
[S] This article contains supplemental Tables S1–S3 and Figs. S1–S3.
ChIP-seq data sets for BRD4 in CD4+ T cells with and without JQ1 treatment, total Pol II in CD4+ T cells with and without JQ1 treatment, Pol II Ser-2 in CD4+ T cells with and without JQ1 treatment, Pol II Ser-5 in CD4+ T cells with and without JQ1 treatment, and BRD4 in hESCs as well as RNA-seq for polyA RNA in CD4+ T cells with and without JQ1 treatment are available in the Gene Expression Omnibus under accession no. GSE33281.

[1] These authors contributed equally to this work.
[2] To whom correspondence should be addressed: Laboratory of Gene Regulation and Inflammation, Singapore Immunology Network (SIgN), Agency for Science, Technology, and Research (A*STAR), Biopolis, Immunos 04-00, 8A Biomedical Grove, Singapore 138648. Tel.: 65-64070006; E-mail: kehchuang_chin@immunol.a-star.edu.sg.

[3] The abbreviations used are: Pol II, RNA polymerase II; P-TEFb, positive transcription elongation factor b; BRD4, bromodomain-containing protein 4; ChIP-seq, ChIP sequencing; hESC, human embryonic stem cell; HAT, histone acetyltransferase; HDAC, histone deacetylase; CBP, CREB-binding protein; CREB, cAMP-responsive element-binding protein; Ab, antibody; UCSC, University of California, Santa Cruz; TSS, transcription start site; RPKM, reads per kilobase of exon model per million mapped reads; DHS, DNase I hypersensitive sites; BET, bromodomain and extraterminal domain nuclear protein.

relative contribution of BRD4 to regulation of Pol II Ser-2 phosphorylation across the genome remains poorly defined.

Although Pol II binding to promoters has been studied extensively, enzyme interactions with enhancer or locus control regions are less well understood (11–14). Recently, Kim *et al.* (15) detected Pol II at enhancers throughout the genome in mouse neurons, but the phosphorylation state of Pol II at these sites was unclear. Ser-5 phosphorylation of Pol II has also been observed at the locus control region of the β-globin gene (11) and Pol II Ser-2 has been detected at the enhancer of the prostate-specific antigen gene (13, 16). We therefore sought to determine whether BRD4 can regulate Pol II activity via Ser-2 phosphorylation at promoters and enhancer regions across the genome.

We analyzed data from ChIP-seq of BRD4 distribution after integration with data describing histone acetylations, methylations, and Pol II binding (17–20) in primary human CD4+ T cells. We report that BRD4 co-localizes with Pol II at promoters and can influence Pol II phosphorylation at Ser-2 at a subset of Pol II-targeted genes. Pol II Ser-2 was decreased at gene bodies upon disruption of BRD4 binding by treatment with the small molecule inhibitor JQ1, and a similar mechanism appeared to characterize enhancer regions. Our data reveal that BRD4 recruitment in human CD4+ T cells occurs predominantly at sites that exhibit H4K5 and H4K8 acetylations. In addition, regions bound by BRD4 and Pol II were enriched in both histone acetyltransferases and deacetylases. Interestingly, we observed that H3K27ac sites bound by BRD4 and Pol II Ser-2 exhibited higher gene activity than H3K27ac sites alone. Our findings indicate that histone hyperacetylation at the promoters and enhancers of transcriptionally active genes contributes to the chromatin environment required for BRD4 binding and may support Pol II recruitment and subsequent phosphorylation at Ser-2. Furthermore, we present evidence that BRD4 occupies different sets of enhancers in CD4+ T cells and in human embryonic stem cells (hESCs), suggesting that BRD4-driven Pol II phosphorylation at serine 2 may play an important role in regulating lineage-specific gene expression.

TABLE 1
Quantitative PCR primers used in the CDK9 ChIP assay

CXCR4 gene	
Primer 1	
Forward	TGTCTGAATTTAGAGGCGGAGGGCGGCGTG
Reverse	GCACAGCTCCGTCGGCCGCACAGAGTTTAA
Primer 2	
Forward	GCGGCCAGAAACTTCAGTTTGTTGG
Reverse	ACTGGACTTACACTGATCCCCTCCATGGTA
Primer 3	
Forward	CGCACGCGCCTCGGTCCCAGCTATCTCC
Reverse	AGTGCTTTCCCCCTCGCGCCACTTCCCTCC
Primer 4	
Forward	ACAGGAGATGAAGTCACTTCGATGACATAA
Reverse	GCTGTTTAGAGAAAGTCTGAAGGCTTACCC
Primer 5	
Forward	CCAAGTAGGGGTAGATAGGCTCTGGGCACC
Reverse	ACCACACTACCAGCACGATTGGCTTTCATC
Primer 6	
Forward	CCTTTTTGCCTCTGTAACAGCCATCTCTCC
Reverse	CCATCTGAAACCACAGTGGGGTGTTAGGTA
FOS gene	
Primer 1	
Forward	TCTGTGTGCTAATCTATGCCCAAATCAACA
Reverse	CAGGAAATCGAATGTAAAACCCTCCGAC
Primer 2	
Forward	GCCACGCTGAAACCTGAAACCATAACGTAA
Reverse	TGAGTTCATGCCGCAAAGGAGAGTCAAG
Primer 3	
Forward	CGTCGCCAGTGTTTGGTGTGTAACGTTCT
Reverse	TGGGAGACAACAACCAAAACAGCAACACAG
Primer 4	
Forward	AACTACTTCTGCATGCTGGGGATGGGCTGT
Reverse	GGCACTTGAAGGAGACCTGACCCCACACTT
Primer 5	
Forward	CCCACGAGACCTCTGAGACAGGAACTG
Reverse	TATGAATGAGTGTAAACGTCACGGGCTCAA
CXCR5 gene	
Primer 1	
Forward	CATGACCTTGTGGTAACCTTGATGTGCCTA
Reverse	ACAGGAAGTGGGGTGGTAAAGGCTGTC
Primer 2	
Forward	GGGTAAACAACCTGAGTGCTGGGGTGATGG
Reverse	CGGGGAGACTGGCAGGAGAGAAGGAGAGA
Primer 3	
Forward	CTCACTCCCTTCCCATAAGCTATAGACCCG
Reverse	CCTGCCTCAGTGTGTTTCTTACACTTCCCT
NANOG gene	
Forward	CAAAATGGAGATACTGATAAGACTTCTTG
Reverse	AGGACACTTTTGTCTAAAATTTTTCAAATA

EXPERIMENTAL PROCEDURES

CD4+ T Cell Isolation, Chromatin Preparation, and ChIP—All blood sample collections and procedures used in this study were approved by the Institutional Review Board of Singapore in accordance with the guidelines of the Health Sciences Authority of Singapore. Informed consent was obtained from all participants in accordance with the Declaration of Helsinki. CD4+ T cells were purified from normal human peripheral blood using the human CD4+ T cell isolation kit II (Miltenyi Biotec). Freshly isolated human CD4+ T cells were treated or not with 500 nM JQ1 for 24 h. The human CD4+ T cells or human embryonic stem cells were sonicated to generate chromatin fragments of ~100–300 bp length. Cells were cross-linked with 1% formaldehyde at room temperature for 7 min prior to sonication. Sonicated chromatin extracts were immunoprecipitated using the anti-BRD4 antibody (Abcam 46199, targeting the amino acid sequence 1348–1362 of BRD4), anti-RNA Pol II Ser-2 (Abcam 5095), anti-RNA Pol II 4H8 (Abcam 5408), and anti-CDK9 (Santa Cruz Biotechnology 484). ChIP assays were performed as described previously (21). Chromatin from 1×10^8 cells (generating ~150–200 μg DNA) was used for each ChIP experiment. Chromatin prepared from different donors were pooled and stored at −80 °C. Five to 10 μg of antibody was used for each ChIP experiment. In the ChIP-seq analyses to determine JQ1 effects, isolated human CD4+ T cells were pooled from five different donors and used for side-by-side experiments of BRD4, Pol II Ser-2, Pol II Ser-5, and total Pol II (4H8) treated with or without 500 nM JQ1 for 24 h. ChIP-enriched DNA was processed and sequenced using Solexa (Illumina) according to the manufacturer's protocol. DNA was sequenced using the Solexa 1G genome analyzer (Illumina) for the BRD4 library, and Genome Analyzer IIx was used to sequence the BRD4 library generated in hESC. The JQ1-treated libraries for BRD4, Pol II Ser-2, and Pol II 4H8 were sequenced on the HiSeq 2000. Fifteen nanograms of each ChIP-enriched DNA were processed for quantitative PCR or for sequencing. The quantitative PCR primers used in the CDK9 ChIP assay were as follows (Table 1).

Alignment of Tag Sequence—ChIP-seq data generated for BRD4 (T cells and hESC) were aligned with the Solexa read

alignment program Eland to reference build hg18 of the human genome. Data for JQ1 comparisons (with and without treatment) for CD4+ T cell poly(A) RNAseq and BRD4, Pol II Ser-2, Pol II Ser-5, and total Pol II (4H8) ChIP-seq were aligned with Bowtie using default parameters and *m* 1, *k* 2, *best*, and *strata*. Mapped sequence tags for Pol II, H3K4me1, H3K4me2, H3K4me3, H2AZ, H3K36me3, H4K20me1, and H3K27me3 generated by ChIP-seq in T cells (data obtained from Ref. 17) were available from the NCBI Short Read Archive under accession no. SRA000206. ChIP-seq data for histone acetylations in T cells (H4K5ac, H4K8ac, H4K12ac, H4K16ac, H3K9ac, H3K14ac, H2AK5ac, H2AK9ac, H2BK12ac, H2BK20ac, H2BK120ac, H2BK5ac, H3K18ac, H3K23ac, H3K27ac, H3K4ac, H3K36ac, and H4K91ac) (19) were downloaded from SRA000287. ChIP-seq data for Ser-5 phosphorylated Pol II and unphosphorylated Pol II were obtained from SRA000234. ChIP-seq data for Ser-2 phosphorylated Pol II was downloaded from GSM501715. ChIP-seq data for histone acetyltransferases (HATs) and HDACs (CBP, p300, p300/CBP-associated factor, males-absent-on-the-first, Tip60, HDAC1, HDAC2, HDAC3, and HDAC6) (20) were downloaded from GSE15735. ChIP-seq data for CD4+ T cell DNase hypersensitive sites were obtained from GSM252783 (22).

Cross-link Co-immunoprecipitation Analysis—Co-immunoprecipitation studies were performed using the Jurkat cell line with the Pierce cross-link IP kit (catalog no. 26147) according to the manufacturer's instructions. Briefly, 5–10 μg of Abs: IgG (Upstate/Millipore), anti-BRD4 (customized and Abcam 75898) and anti-CDK9 (Santa Cruz Biotechnology, sc-484) were coupled to protein A/G-agarose by incubation for 1 h at room temperature. The bound Abs were then cross-linked with disuccinimidyl suberate for 1 h at room temperature. Jurkat cells were lysed in lysis buffer (25 mM Tris, pH 7.4, 150 mM NaCl, 1% Nonidet P-40, 1 mM EDTA, 5% glycerol, and protease inhibitor mixture), followed by preclearing with Pierce control resin to reduce nonspecific binding. The samples were incubated with Ab-cross-linked resin in the column overnight at 4 °C. Immunoprecipitates were washed three times with lysis buffer and once with conditioning buffer (neutral pH buffer). The resulting antigens were eluted with elution buffer (primary amine, pH 2.8) and then diluted with 5× sample loading buffer. Proteins were subjected to SDS-PAGE followed by Western blot analysis.

Peptide Competition Assay—Four identical samples (Jurkat or HeLa cell lysate prepared as described in "Cross-link Co-immunoprecipitation Analysis") were prepared for analysis of each antibody (S2 RNAPII, ab5095; S2 RNAPII H5, ab24758). Proteins from each cell line were transferred and immobilized on a PVDF membrane. At the same time, 4 ml of primary antibody (1 μg/ml) was prepared in nonfat milk blocking buffer, and the individual peptides (RNAPII carboxy-terminal domain repeats YSPTSPS peptide ab12795, RNAPII carboxy-terminal domain repeats YSPTSPS phospho-Ser-5 ab18488, RNAPII carboxy-terminal domain repeats YSPTSPS phosphor-Ser-2 ab12793, respectively), were added to achieve 200-fold molar excess of peptide to antibody. The antibodies, preincubated or not with specific peptides, were then incubated with each sample for 2 h at room temperature. After several washes to remove unbound antibody, secondary antibodies (goat anti-rabbit IgG-HRP or goat anti-mouse IgM-HRP) were added prior to further incubation. Unbound secondary antibodies were then removed by thorough washing before the bands were developed.

TABLE 2
Region-type definitions and score for peak-gene associations

Region	Definition	Score
Proximal promoter	−2 kb to 0 b upstream of TSS	2
Distal promoter	−10 kb to − 2 kb upstream of TSS	1
5′ Distal	−50 kb to − 10 kb upstream of TSS	0
>50 kb upstream	Greater than − 50 kb upstream	0
First exon	Within first exon	2
Other exon	Within exons other than first exon	2
Intronic	Intragenic regions other than exons	2
3′ Proximal downstream	Within 1.5 kb downstream of TTS	2
3′ Distal downstream	Within 1.5 kb to 50 kb downstream of TTS	0
>50 kb downstream	Greater than 50 kb downstream of TTS	0

Peak Calling—Peak calling was performed using FindPeaks4 (23) with a 200-bp extension of sequence tags and a false discovery rate of 0.01 (using the Lander-Waterman algorithm). Sequenced tags were excluded from peak calling if they were either duplicate reads, reads with >2 ambiguous base calls, or >2 mapping mismatches. ChIP-seq libraries used in the analysis of effects of JQ1 on BRD4 and different phosphorylation states of Pol II were called with a false discovery rate of 0.0000001 due to their high sequencing depth. See supplemental "Methods" for identification of peak gene associations, classification of peak binding region, and determination of peak binding overlap.

Peak Gene Association—The peaks belonging to a library were first overlaid with refseq transcripts in the refFlat table (build hg18, extended by 50 kb) downloaded from the University of California, Santa Cruz (UCSC). Overlap with the extended refseq transcripts was determined using intersectBed from BEDTools (version 2.16.2) (24). Only the peak-gene overlaps that involved at least 50% of the width of the peak were retained for classification of peak binding region.

Classification of Peak Binding Region—Peak-gene associations were used to classify BRD4 binding region type by calculating the distance from the BRD4 peak max to the transcription start site (TSS) and termination site of the gene.

Region-type Definitions and Score for Peak-gene Associations—Peak-gene association analysis was performed using the Perl Programming Language (version 5.10.0) (Table 2). Peak-gene associations were identified only where association scores were equal to the maximum obtained for a particular peak.

Peak Binding Overlap/Co-localization—Unless otherwise stated in the text, overlap was defined as ≥1 bp of a histone modification or Pol II peak that occurred within ±1 kb of the BRD4 peak max. Overlap of BRD4 binding in CD4+ T cells and hESCs was defined as ≥1 bp of a BRD4 peak in hESCs that occurred within ±2.5 kb of a BRD4 peak max in CD4+ T cells.

CpG Islands—Genomic coordinates of CpG islands table "cpgIslandExt" for hg18 were obtained from the UCSC Table Browser.

Tag Density Distribution—Sequence tags that contributed to statistically significant peaks were extracted and directionally extended by 200 bp. Tag density distributions were then plotted in windows centered on either the TSS for promoters or on

BRD4 peak max position for non-promoters. Total tags in 50-bp bins were then counted for each window.

Tag density profiles were obtained by calculating the average normalized tag count for all genes/sites analyzed in each bin. For each gene analyzed, tag density distributions in the transcript width were counted for bin sizes 1/100 of the length of the gene body.

Tag Normalization—For comparisons between libraries, tag counts in each bin were normalized by a factor of 10/("*n*"; number of million non-duplicate mapped tags in the library, calculated to two decimal places). The value *n* number of million non-duplicate mapped tags reflects the number of tags used for peak calling.

Tag Density Heat Maps—Heat maps were generated from matrices of calculated tag density distribution and visualized using Java TreeView (25). Contrast value 3 was used for all heat maps except H3K36me3 (1.01), H3K27me3 (0.3), and CpG (0.81).

Nucleosome Preparation—Jurkat T cells were lysed in lysis buffer (20 mM HEPES (pH 7.3), 3 mM $MgCl_2$, 0.25 M sucrose, 0.5% Nonidet P-40) and then washed twice in fresh lysis buffer. The cell pellets were resuspended in buffer B (20 mM HEPES, 3 mM $MgCl_2$, 0.2 mM EGTA). Three mg of DNA was used for each reaction of oligonucleosome generation. An equal volume of buffer B containing an additional 0.6 M KCl and 10% glycerol was then added and incubated for 30 min at 4 °C. The nuclear pellets were obtained by centrifugation at 17,000 × *g* for 40 min and were subsequently resuspended in digestion buffer (20 mM HEPES, pH 7.3, 10 mM KCl, 1.5 mM $MgCl_2$, 0.34 M sucrose, 2 mm $CaCl_2$, 10% glycerol). Chromatin was digested with micrococcal nuclease (Worthington) at 37 °C for 15 min (50 units/mg DNA in a total volume of 400 μl). The reaction was stopped by addition of 5 mM EGTA and centrifugation at 600 × *g*. The nuclear pellets were resuspended in nuclear extraction buffer (20 mM HEPES, pH 7.35, 420 mM NaCl, 1.5 mM $MgCl_2$, 0.2 mM EGTA) and kept on ice for 1 h. Nuclear debris was removed by centrifugation (1000 × *g* for 5 min at 4 °C). The salt concentration of the supernatant was then adjusted to 150 mM NaCl by addition of dilution and equilibration buffer (20 mM HEPES, pH 7.35, 1.5 mM $MgCl_2$, 0.2 mM EGTA, and 25% glycerol), whereas the supernatant was vortexed. The resulting H1-chromatin-enriched precipitate was cleared by centrifugation, and the suspension containing mainly mononucleosomes and dinucleosomes was used for GST pulldown (see below).

Glutathione S-Transferase (GST)-BD1 and -BD2 Nucleosome Pulldown Assay—Purified GST, GST-BD1, and GST-BD2 proteins were incubated overnight at 4 °C under gentle rotation with mononucleosomes in a total volume of 500-μl binding buffer (50 mM Tris, pH 7.4, 100 mM NaCl, 0.1% Nonidet P-40, 10% glycerol). Following incubation, glutathione-Sepharose 4 Fast Flow beads were added to the reaction and incubated for 2 h at 4 °C. Beads were washed five times with binding buffer, resuspended in 2× sample loading buffer, heated for 5 min at 95 °C, and then analyzed by SDS-PAGE and Western blotting.

H3 and H4 Peptide Binding Assay—Ten micrograms of GST-purified BD1- and BD2-BRD4 proteins were incubated overnight at 4 °C with 0.02 μg of N terminus biotin-labeled synthetic H3 or H4 peptides carrying acetylation or methylation modifications at specific lysine residues (or with control peptides that lacked modifications) in a buffer containing 50 mM Tris-HCl, pH 7.4, 15 mM $MgCl_2$, 150 mM NaCl, 0.5 mM DTT, and 0.1% Nonidet P-40. The following day, 25 μl of M-280 streptavidin beads (Dynal) were added to the peptide mixture and incubated for 1 h at 4 °C. The beads were washed three times before the bound proteins were eluted with 2× sample buffer and resolved by SDS-PAGE for Western blotting.

TABLE 3
RT-PCR primers used in this work

CXCR4	
Forward	CCCGACTTCATCTTTGCCAACGTCAGTGAG
Reverse	TCTGGTGGCCCTTGGAGTGTGACAGCTT
RUNX3	
Forward	GCAGGCAATGACGAGAACTA
Reverse	GTCTGGTCCTCCAGCTTCTG
CD4	
Forward	TTCCCTCCACAGTGACTGCCAACTCTGA
Reverse	CAAGACAGTGCATGTCCAGGTGCCACTATC
IL2RA	
Forward	GAACCATGTTGAACTGTGAATGCAAGAGAG
Reverse	TTGCATTTCTGTGGTTTTCCTTTCTTTCTG
FOS	
Forward	GTCTCCAGTGCCAACTTCATTCCCACGGTC
Reverse	GCTCGGCCTCCTGTCATGGTCTTCACAAC

Western Blots—For antibody specificity assays, HeLa and Jurkat cell lines were seeded at a density of 5 × 105 cells/well in a six-well plate. Twenty four hours after seeding, the cells were treated or not with Flavopiridol at the indicated concentrations (0.01–1 μM) for 1 h. The cells were then lysed and subjected to Western blot analysis. Western blots were carried out using standard protocols. Antibodies used were CDK9 (Santa Cruz Biotechnology, sc484), BRD4 (Abcam, 75898, and customized Ab against epitope sequence NFQSDLLSIFEENLF at the C-terminal of BRD4 protein), RNA Pol II phospho-Ser-2 H5 (ab24758), S2 RNA Pol II phospho-Ser-2 (ab5095), RNA Pol II phospho-Ser-5 (ab5131), RNA Pol II 4H8 (ab5408), and actin (Chemicon MAB 1501). HRP-conjugated secondary antibodies used were anti-rabbit IgG (GE Healthcare, NA934V), anti-mouse IgG (GE Healthcare, NA931V), anti-mouse IgM (Santa Cruz Biotechnology, sc2064), and anti-protein A (GE Healthcare, NA9120V).

RNA Isolation, Quantitative RT-PCR Analysis, and RNA-seq—Human CD4+ T cells were treated or not with 1000 nM JQ1 for 24 h. Total RNA was extracted using TRIzol (Invitrogen) and purified by an RNeasy mini kit (Qiagen). RNA concentration was quantitated using a NanoDrop spectrophotometer (Thermo Scientific). For cDNA synthesis, 1 μg of total RNA was used with the SuperScript II kit (Invitrogen) according to the manufacturer's instructions. RNA levels were measured by real-time PCR using SYBR Green detection with the ABI Prism 7900HT machine (Applied Biosystems). Results were normalized to GAPDH. RNA sequencing was performed using an Illumina GA IIX next-gen sequencer. The image processing and base calling were performed by real-time analysis. RT-PCR primers are shown in Table 3.

Calculation of RNA-seq Transcript Expression and Definition of JQ1-sensitive Refseq Transcripts—Uniquely mapped reads with a maximum of two ambiguous base calls and a maximum of two base mismatches were used for transcript expression measurements. A total of 24,083,771 reads was obtained from

TABLE 4
***p* values and adjusted *p* values from pairwise Wilcoxon rank sum tests between four classes of transcripts**

Group 1	Group 2	*p* value	Adjusted *p* value
BRD4/H3K27ac overlapping sites	BRD4 unique sites	1.18×10^{-307}	7.10×10^{-307}
BRD4/H3K27ac overlapping sites	H3K27ac unique sites	1.01×10^{-54}	6.04×10^{-54}
BRD4/H3K27ac overlapping sites	DHS unique sites	0	0
BRD4 unique sites	H3K27ac unique sites	1.90×10^{-34}	1.14×10^{-34}
BRD4 unique sites	DHS unique sites	0.76	1
H3K27ac unique sites	DHS unique sites	1.38×10^{-46}	8.27×10^{-46}

the non-treated CD4+ T cell poly(A) RNA library, and 26,361,151 reads were obtained from the JQ1-treated CD4+ T cell poly(A) RNA library. Estimation of refseq transcript expression was performed using the Partek Genomics Suite™ RNA-seq workflow (Partek® software, version 6.5, build 6.11.0121). Transcript level mapping was performed using 28,787 transcripts of the hg18 refGene table, downloaded from USCS Table Browser (6). Reads per kilobase of exon model per million mapped reads (RPKM) values were used for further analysis. Transcripts that displayed RNA-seq expression values of ≥5 RPKM that were decreased by half or more upon JQ1 treatment were regarded as being down-regulated by JQ1.

Percentage of BRD4 Binding for RNA-seq Transcript Expression Categories—Refseq transcripts were categorized based on their RPKM values into the following 12 expression categories: 0 RPKM; less than or equal to 1, 2, 3, 4, 5, 6, 7, 8, 9, 10 RPKM; and greater than 10 RPKM. Transcripts were considered to be BRD4-bound if they had been associated to a BRD4 peak through peak-gene association and classification of binding region.

Test of Correlation for BRD4 Peak Height with Transcript Expression—All transcripts were first ranked according to their RPKM expression levels and binned into groups of hundreds. The average height of the 100 BRD4 peaks in each bin was calculated, and a test for correlation between average peak height and bin expression number was performed using the Spearman's correlation coefficient. The Spearman correlation of $\rho = 0.848$ was obtained.

Pearson's Chi-squared Test for BRD4 Binding Regions Compared with Randomized Binding Regions—Control distributions were generated from 1000 sets of BRD4 peaks placed randomly across the genome (shuffleBed, BEDTools, version 2.16.2 (24)). Peak-gene association and classification of binding regions for each set of 33,544 peaks was then conducted. Pearson's Chi-squared test was subsequently used to compare the distribution of actual BRD4 peaks with the mean distribution of the randomized data sets across the following gene regions; first exon, proximal promoter, 3′ proximal downstream, other exon, distal promoter, intronic, 5′ distal, 3′ distal downstream, >50 k downstream, >50 k upstream, and "not associated." The ratio of experimentally observed BRD4 peaks to randomized control peaks was then calculated for each gene region. The *p* values shown in Fig. 2*B* represent the probability of observing, by chance, a higher number of peaks in that region than was detected experimentally by BRD4 ChIP-seq. For the not associated region, *p* values describe the probability of observing, by chance, a lower number of peaks in that region than was detected experimentally by BRD4 ChIP-seq.

Comparison of RPKM between Groups of Refseq Transcripts—Refseq transcripts were grouped into four classes based on their association with BRD4, H3K27ac, or DNase I hypersensitive sites (DHS). A non-parametric analysis of variance (Kruskal-Wallis rank sum test) was performed in R, a language and environment for statistical computing and graphics, using the function "kruskal test" where $p < 2.2 \times 10^{-16}$ indicated that medians were significantly different. Pairwise Wilcoxon rank sum test was used to compare transcript classes using the R function "wilcox test." *p* values were adjusted with a Bonferroni correction using the R function "p.adjust" (Table 4).

Pathway Enrichment Analysis—Pathway enrichment analysis was performed using IPA software (Ingenuity® Systems) to obtain the negative log *p* values of gene enrichment in different canonical pathways.

RESULTS

BRD4 Binding Is Associated with Active Genes across the Genome—To establish whether BRD4 regulates transcription elongation in a genome-wide manner, we performed ChIP followed by DNA sequencing in primary human CD4+ T cells to identify 33,544 BRD4 binding sites (peaks). The specificity of the BRD4 antibody (Abcam 46199) was confirmed by Western blotting using the total lysate, cytoplasmic lysate, and nuclear lysate of THP-1 and HeLa S3 cells. The BRD4 antibody routinely detected a protein of the appropriate molecular weight for BRD4 (~250 kDa; supplemental Fig S1*a*) (10, 26). We first examined two individual active loci in CD4+ T cells; both *CD4* and *LCK* exhibited high levels of BRD4 binding not only in promoter regions but also in multiple intergenic and intronic regions (Fig. 1*A*). Conversely, inactive loci *IL13* and *IL5* (silent genes in non-polarized T cells) lacked occupancy by BRD4 (Fig. 1*B*). To determine whether these findings were indicative of a broader trend in transcriptional regulation, we examined the relationship between BRD4 sites and levels of gene expression on a global scale. Gene expression levels were measured by high-throughput sequencing of polyadenylated RNA from human CD4+ T cells. We observed that the majority of expressed genes (81.8%) were targets for BRD4 binding (23,518 transcripts with RPKM ≥1) and that this feature was particularly evident among highly expressed genes (Fig. 1*C*). To verify the relationship between gene expression and BRD4 binding, Refseq transcripts were ranked by RPKM value (with the order of ties selected randomly and then grouped into bins of 100 transcripts. Pearson's Chi-squared test was used to analyze the 28,787 transcripts based on their bin number and presence or absence of BRD4. We observed significant dependence between levels of gene expression and the presence of BRD4 (X-squared = 9255.312, $df = 287$, $p < 2.2e^{-16}$). A similar analysis of transcript associations with Pol II (supplemental Fig S1*b*) and H3K4me3 (supplemental Fig S1*c*) displayed a comparable trend, indicating that increased transcript expression was asso-

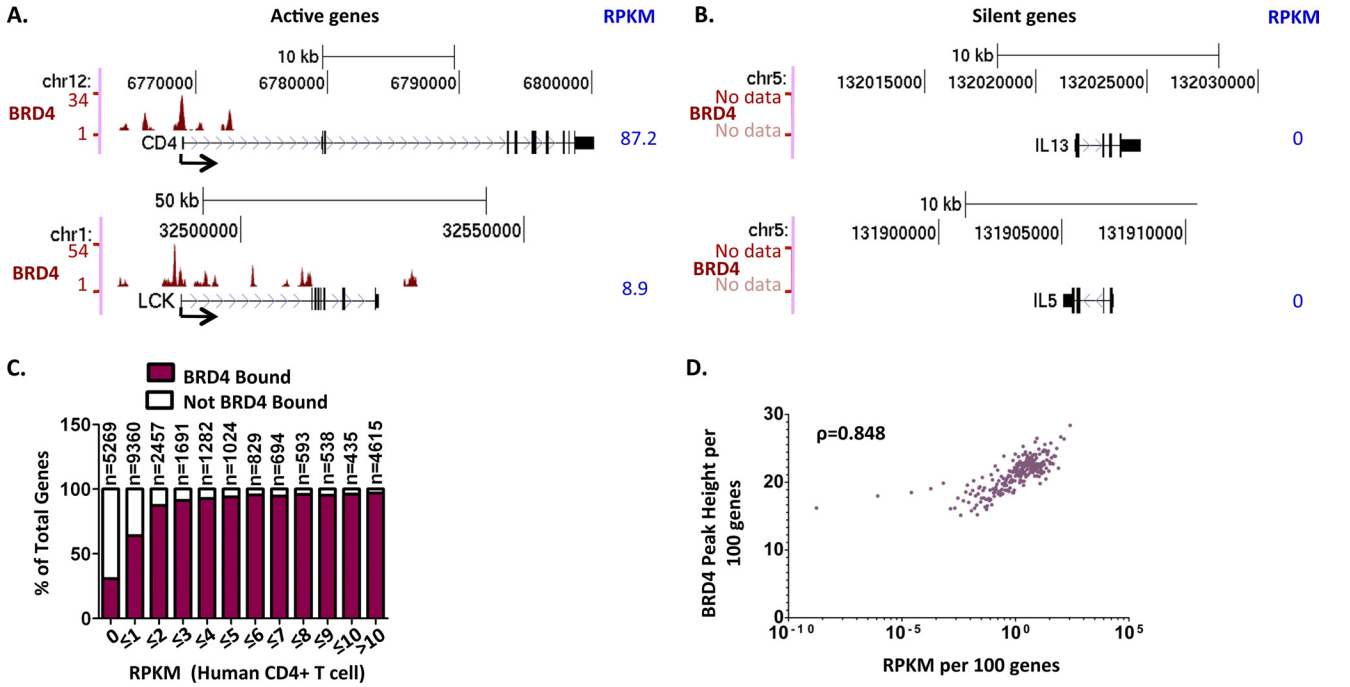

FIGURE 1. **BRD4 binding is associated with active genes across the genome.** UCSC genome browser views of BRD4 ChIP-seq peaks identified at active genes *CD4* (*top*) and *LCK* (*bottom*) with 87.2 and 8.9 RPKM respective expression levels as assessed by RNA-seq (*A*); silent genes *IL13* (*top*) and *IL5* (*bottom*) with 0 RPKM expression as assessed by RNA-seq (*B*). *C*, Refseq transcripts were categorized according to RNA-seq RPKM expression levels (*x* axis), and the relative proportion of transcripts in each category (*y* axis) with BRD4 targets were identified by the *maroon* color. *D*, average BRD4 peak height was calculated for bins of 100 transcripts each and then analyzed by Spearman correlation. Average BRD4 peak height is shown against RPKM expression per 100 genes (transcripts are sorted by expression values). Spearman correlation was $r = 0.848$ (see also supplemental Fig. S1).

ciated with the increased presence of Pol II and H3K4me3. Moreover, from a Spearman correlation test of RPKM and peak height, we found gene expression levels were strongly correlated with BRD4 peak height (ρ, 0.848; $p < 0.0001$; Fig. 1*D*). Taken together, these data indicate that genome-wide binding of BRD4 is associated with active genes and that levels of BRD4 binding correlate with gene expression activity.

BRD4 Binds Both Promoters and Enhancers—To further clarify the role played by BRD4 in global transcriptional regulation, we examined the distribution of BRD4 binding sites within the gene that encodes chemokine receptor 4 (*CXCR4*); a protein that influences T cell migration and may support HIV cell entry (27). We identified BRD4 peaks in multiple regions along the *CXCR4* gene and promoter (Fig. 2*A* and supplemental Fig S2*a*). These regions displayed high levels of the H3K4me3 mark of transcription initiation that is generally found located within promoters (17, 19). Intriguingly, peaks of BRD4 binding were also detected 7–24 kb upstream of the TSS for *CXCR4* (Fig. 2*A*, *right box*). These BRD4 binding regions co-localized with H3K4me2 and H3K4me1, which are often enriched at gene enhancers (19, 28). Lower levels of H3K4me3 were also detected in a region upstream of the TSS, consistent with reports from other investigators (17). Further analyses revealed additional BRD4 binding capacity in the upstream regions of other genes expressed in T cells, including *FOS*, *BCL3*, and *CXCR5* (supplemental Fig S2, *b*, *c*, and *f*, respectively). Known enhancer elements, including the proximal enhancer and thymocyte enhancer regions of the *CD4* gene, as well as the Positive Regulatory Region IV and CD28RE regions of *IL2RA* (as defined in Ref. 29), were also found to exhibit BRD4 binding sites (supplemental Fig. S2, *d* and *e*, respectively). These data indicated that BRD4 binds both to promoters and enhancers and potentially associates with *cis*-acting regulatory elements that may influence transcription across the genome.

To assess the extent of BRD4 binding at promoters and regulatory elements, we next examined the distribution of BRD4 peaks across the genome with respect to individual genes (Fig. 2*B*). Although single gene studies have previously suggested that BRD4 acts primarily at promoters (8, 10), other studies have reported detection of the BRD4-CDK9 complex at the enhancer of the FOSL1 gene (9) and BRD4 binding at the IgH enhancer in MM.1S cells (30). In our genome-wide analysis, we observed that only ~20% of BRD4 binding sites were located in proximal promoters. More than half of the BRD4 binding peaks occurred within intergenic and intragenic regions, with the majority of these being situated in introns and the first exon (Fig. 2*B*). BRD4 binding at the gene regions defined in Fig. 2*B* was significantly different from the distribution of 1000 random BRD4 sites sampled from across the genome (X-squared = 14490.58, df = 10, p value $< 2.2 \times 10^{-16}$). The BRD4 binding peaks identified by ChIP-seq for each of the gene regions analyzed were also substantially higher than those observed among the 1000 randomized BRD4 binding sites (supplemental Fig S2*g*). Notably, the first exon and proximal promoter displayed the highest ratio of observed to expected BRD4 binding peaks (38.75 and 16.90, respectively; supplemental Fig S2*g*). The non-random binding of BRD4 across the genome suggests a targeted role for this protein in regulating gene expression.

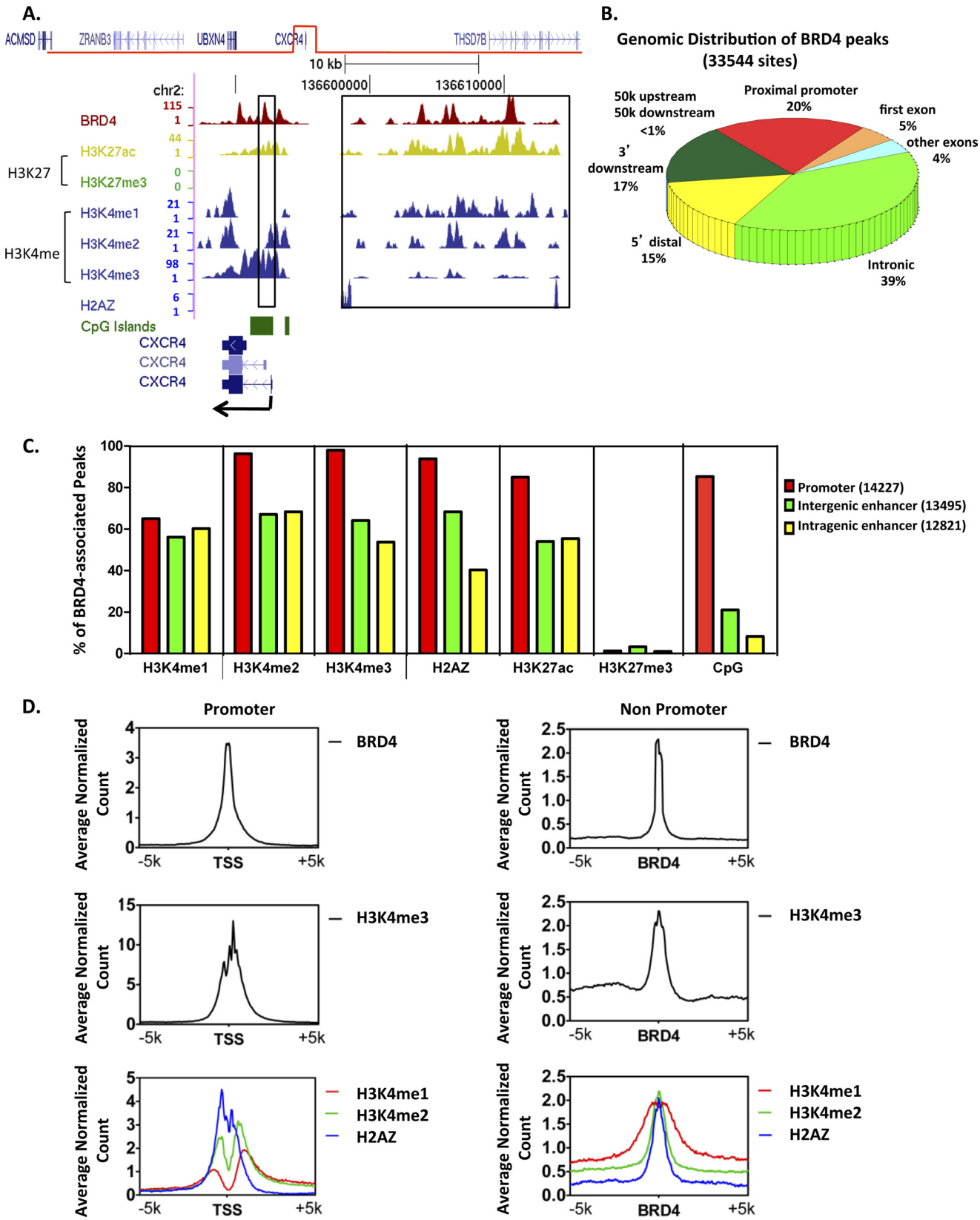

FIGURE 2. **BRD4 binding occurs at both promoters and enhancers.** *A*, UCSC genome browser view of chromatin modification patterns (data obtained from Refs. 17 and 19) as well as BRD4 distribution and CpG islands at the *CXCR4* gene locus. Binding and histone modifications observed at the promoter (*left black box*) and enhancer region 7–24 kb upstream (*right black box*) are shown. *B*, locations of BRD4 peaks relative to gene annotations. *C*, the percentage of BRD4 peaks associated with different histone modifications and CpG islands was calculated for promoter, intergenic, and intragenic regions by assessing overlap of the histone mark with the 1 kb region flanking the BRD4 peak max. *D*, average normalized tag counts for BRD4 (*top panel*), H3K4me3 (*middle panel*), and H3K4me1, me2, H2AZ, and H3K27me3 (*bottom panel*) in 10-kb windows centered on the TSS of all BRD4-associated refseq transcripts (*left*, promoter) and 10-kb windows centered on the BRD4 peak max position at all enhancer BRD4 binding sites (*right*, non promoter) (see also supplemental Fig. S2).

Although no single histone modification pattern can unambiguously define all enhancer elements, these patterns do reportedly include all three H3K4 methylation states (H3K4me1, H3K4me2, and H3K4me3) (31) as well as the histone variant H2A.Z (17). Enhancers can also be characterized by the presence of high levels of H3K4me1 combined with low levels of H3K4me3 (17). In our analyses, histone variant H2A.Z and all three methylated forms of H3K4 could be detected in association with BRD4 (Fig. 2*C*). To ascertain that the BRD4 binding sites we defined as enhancers were not simply undefined promoters, we next divided these sites into three categories relative to annotated refseq transcripts ("promoter," "intergenic," and "intragenic") and compared the histone modification patterns in each group. Promoter binding sites were defined as peaks that occurred within ±2 kb of an annotated TSS, intragenic binding sites were located within the gene body but outside the 2-kb region flanking the TSS, and intergenic binding sites were peaks outside of the gene body and >2 kb distant from the TSS. The incidence of histone modification H3K4me1 in the BRD4 binding sites were comparable between the promoters, intergenic, and intragenic regions, whereas H3K4me2, H3K4me3, and H2A.Z overlapped with 80–100% of promoters, but with only 40–65% of other sites (Fig. 2*C*). The average tag count for H3K4me3 was 5-fold lower in non-promoter sites compared with promoter sites (Fig. 2*D*, *middle panel*). In addition, these histone marks showed a distinct multimodal distribution at promoter sites but not at enhancer sites, consistent with reports that nucleosomes are depleted at the TSS (19). Another distinguishing factor was that signal strength for BRD4 binding at the average promoter was ~1.5-fold higher than that observed for the average enhancer (Fig. 2*D*, *top panel*).

CpG islands are enriched in ~72% of human promoters and have been used to distinguish promoters from enhancers (32). We detected CpG islands in 85% of the promoters that included BRD4 binding sites, whereas only 21% of the intergenic regions and 8% of the intragenic regions with BRD4 binding sites incorporated CpG islands (Fig. 2*C*). Together, the histone and CpG analyses confirmed that the regions bound by BRD4 and defined here as enhancers are not unannotated promoters.

The repressive histone marker H3K27me3 overlapped poorly with BRD4 binding sites at both promoters and enhancers (Fig. 2*C*). In contrast, the active histone mark H3K27ac was prevalent at BRD4 binding sites (Fig. 2*C*). These findings are consistent with the observation that BRD4 primarily targets active genes (Fig. 1*C*). We observed that 65.7% of the 23,518 transcripts with RPKM ≥1 exhibited BRD4 binding at the promoter, and a further 54.5% of these genes also bound BRD4 at enhancer elements. These data illustrated that BRD4 binding to promoters and enhancers is shared by the majority of active genes.

BRD4 and Pol II Co-localize at Enhancers and Promoters—At the *CXCR4* gene, binding peaks for both Ser-5- and Ser-2-phosphorylated Pol II co-localized with BRD4 at multiple regions along the gene, the promoter, and at a region 7–24 kb upstream of the TSS (Fig. 3*A*). Similar co-localization of BRD4 with phosphorylated Pol II was also observed at the *FOS* gene and corresponding upstream region (Fig. 3*B*). These data led us to examine the genome-wide relationship between BRD4 and Pol II (using data obtained from Ref. 17). Of the 11,964 Refseq genes in our analyses that were found to be associated with Pol II, 11,333 of these genes (95%) were also associated with BRD4 (supplemental Fig. S3*a*). Furthermore, 54% (18,244) of the BRD4 binding sites displayed a Pol II peak within 1 kb of the BRD4 peak max (FigS 3b), indicating that a substantial number of BRD4 and Pol II binding sites are co-localized.

Further analysis in human CD4+ T cells confirmed that BRD4, Pol II, and Pol II Ser-2 co-occupied promoters across the genome. The specificity of the antibody against Ser-2 phosphorylation (ab5095) as used for the ChIP-seq analysis (data from Ref. 18), was confirmed by comparison with an alternative antibody (H5) against phosphorylated Ser-2 (supplemental Fig S3, *c* and *d*). Among all 29,658 Refseq transcript promoters, 95% of the Pol II-bound loci and 96% of the Pol II Ser-2-bound loci displayed BRD4 co-binding within the same 10-kb window centered on the TSS (Fig. 3*C*). Consistent with the notion that BRD4 associates with active gene expression, BRD4 and Pol II sites were enriched in the activation marks H3K27ac, H4K20me1, and H3K36me3. In addition, marks H4K20me1 and H3K36me3 are associated with actively transcribed regions of genes, with high levels of these variants being found at the TSS and transcription termination site, respectively (17). Sites at which BRD4 and Pol II co-localized exhibited substantial levels of the marks H3K4me3 and H3K9ac that are known to associate with Pol II binding (33). In contrast, the repressive mark H3K27me3 was observed primarily at TSS that lacked BRD4 and Pol II binding.

In approximately half of cases, the 10-kb analytical windows centered on BRD4 peak max at enhancers also exhibited Pol II and Pol II Ser-2 binding (Fig. 3*D*). H3K27ac was enriched in this subset of enhancers that displayed dual binding of Pol II and BRD4, whereas H3K27me3 levels were low or were not detected at these sites. If the presence of BRD4 at enhancers was determined by enhancer-promoter interactions, the enhancer would be expected to display promoter BRD4 peaks, and these regions should co-precipitate by ChIP. However, we detected 58 genes that displayed Pol II Ser-2 only at promoters, whereas BRD4 binding was present only in enhancer regions (supplemental Fig. S3*e* and supplemental Table S1). These data suggested that at least one mechanism of BRD4 association with enhancers is due to direct binding. In 384 genes, Pol II Ser-2 was present at enhancers but not at promoters (supplemental Fig. S3*f* and supplemental Table S2), suggesting that Pol II can bind to enhancers independently of promoter regions.

BRD4 Association with Histone Acetylation Marks—Although BRD4 binding depends on acetylated histones, it is unclear which patterns of histone acetylation can favor BRD4 binding across the genome. In the current report, BRD4 binding sites upstream of the *CXCR4* and *FOS* genes clearly co-localized with a specific combination of histone acetylations (supplemental Fig. S2, *a* and *b*). BRD4 binding has been reported to occur at peptides H3 (lysines K9/14), diacetylated H4 (lysines K5/12), and at tetra-acetylated H4 (K5/8/12/16) *in vitro* (7). Data from *in vivo* studies have also identified H4 (K5/8/12) (8), H3 (K9acS10ph), and H4 (K16ac) (9) acetylation patterns as capable of promoting BRD4 binding. We therefore

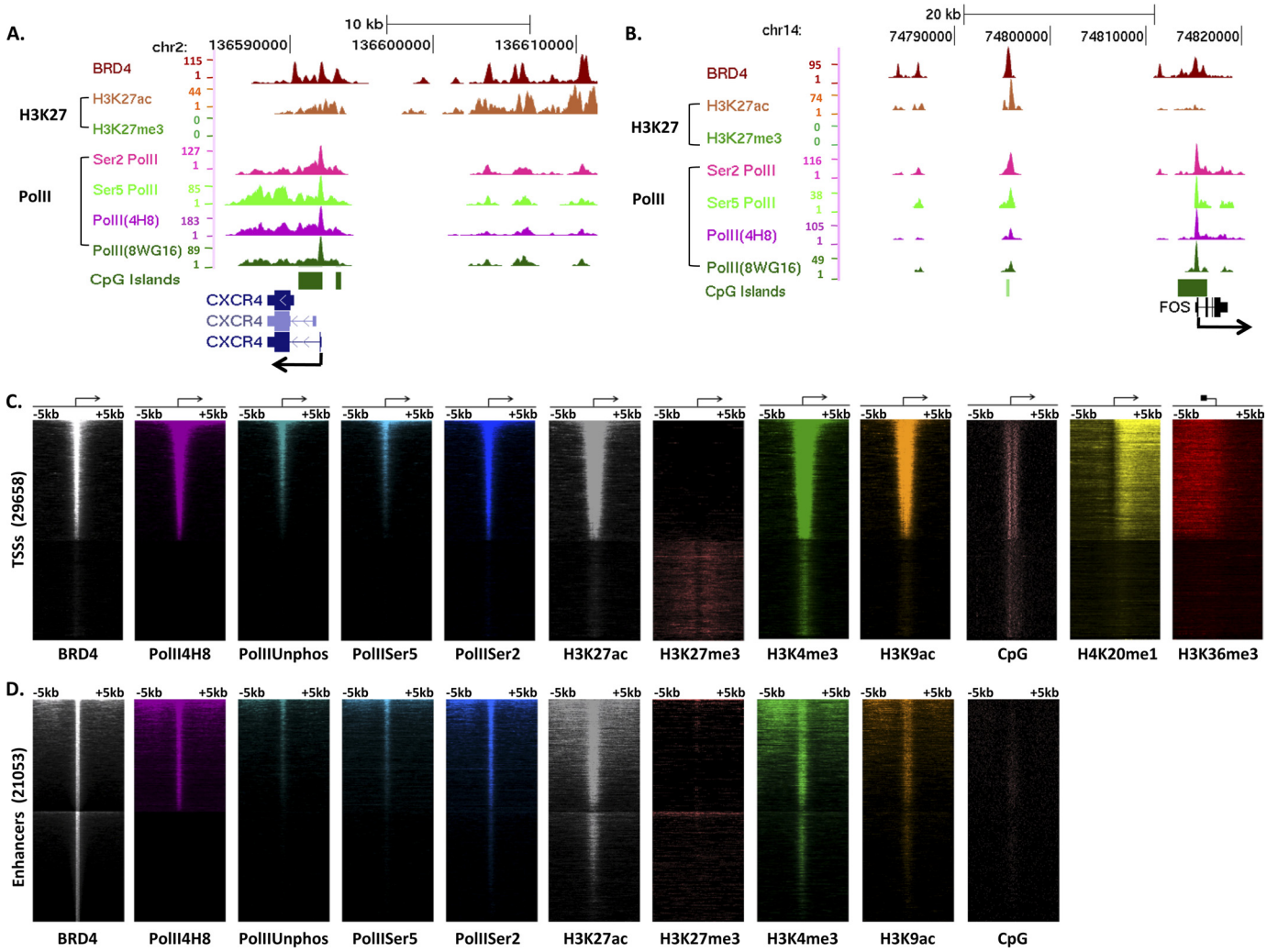

FIGURE 3. **BRD4 and Pol II co-localize at promoters and enhancers.** UCSC genome browser view of chromatin modification patterns, different phosphorylated Pol II (*PolII*) states, BRD4 and CpG islands at the *CXCR4* gene locus (*A*), and the *FOS* gene locus (*B*). *C*, heat map illustrating normalized tag counts for BRD4, different phosphorylated states of Pol II, histone marks, and CpG islands in 10-kb windows centered on the TSS of 29,658 Refseq transcripts. *Windows* in each panel were ordered by decreasing Pol II 4H8 tag levels. CpG islands were given artificial tag counts. Image contrast was set to three for all heat maps except for CpG (0.81), H3K27me3 (0.3), and H3K36me3 (1.01). *D*, heat map representation in 10-kb windows centered on the BRD4 peak max positions of 21,053 enhancer BRD4 binding sites. *Windows* in each panel were ordered by decreasing Pol II 4H8 tag levels. Image contrast settings for all heat maps were the same as in *D* (see also supplemental Fig. S3). *Unphos*, unphosphorylated.

sought to identify the histone acetylation patterns that facilitate BRD4 binding at a genomic level. To this end, we integrated global BRD4 binding site data with acetylation data for histones H4 and H3 across the entire genome (using data from Ref. 19). H4K5 and H4K8 acetylations were each found to be associated with more than 50% of BRD4 binding sites (Fig. 4*A*). Although 35% of BRD4 binding sites did not exhibit any combination of the four predominant H4 acetylations (K5, K8, K12, K16; Fig. 4*B*, *striped bar*), the majority of BRD4 binding sites were preferentially associated with H4K5 and H4K8 acetylations (Fig. 4*B*, *black bars*). H4 di- and triacetylated regions that lacked K5 and K8 acetylation rarely co-occurred with BRD4 binding sites (Fig. 4*B*, *white bars*). Furthermore, *in vitro* assays demonstrated that BRD4 (Fig. 4*C*) subdomain BD1 but not BD2 interacted with K5 and K8 acetylations of H4 in the native mono-nucleosome of Jurkat T cells (Fig. 4*D*).

To confirm that the histone acetylation patterns enriched at BRD4 binding sites in primary human CD4+ T cells (Fig. 4*B*, *black bars*) did indeed facilitate BRD4 binding, peptides with combinations of H4 or H3 acetylations (Fig. 4*E*) were used to probe for BD1 binding *in vitro*. BD1 failed to bind non- or monoacetylated H4 (Fig. 4*F*, *lanes 2–4*, and Fig. 4*H*, *lanes 2* and *3*) or to H3 tail peptides (Fig. 4*G*, *lanes 2–4*). Individual histone acetylation H4K5 and H4K8 tail peptides were not sufficient for BD1 binding *in vitro*, despite the observed enrichment in *in vivo* binding to these sites. These data perhaps indicated a requirement for additional histone acetylations to support BRD4 binding. BD1 bound to acetylated peptides H4K5/8 (Fig. 4*F*, *lane 5*, and Fig. 4*H*, *lane 9*), H4K5/12 (Fig. 4*H*, *lane 11*), and H3K9/14 (Fig. 4*G*, *lanes 5* and *7*). However, H4K5/12ac (Fig. 4*B*) and H3K9/14ac (data not shown) were not globally enriched at BRD4 binding sites. Triacetylated H4 peptides (Fig. 4*F*, *lanes 6* and *7*, and Fig. 4*H*, *lanes 17* and *18*) and tetra-acetylated H4 peptides (Fig. 4*F*, *lane 8*) that included both K5 and K8 acetylations also interacted with the BD1 domain, consistent with the *in vivo* data. Thus, H4K5/8ac, either alone or in combination

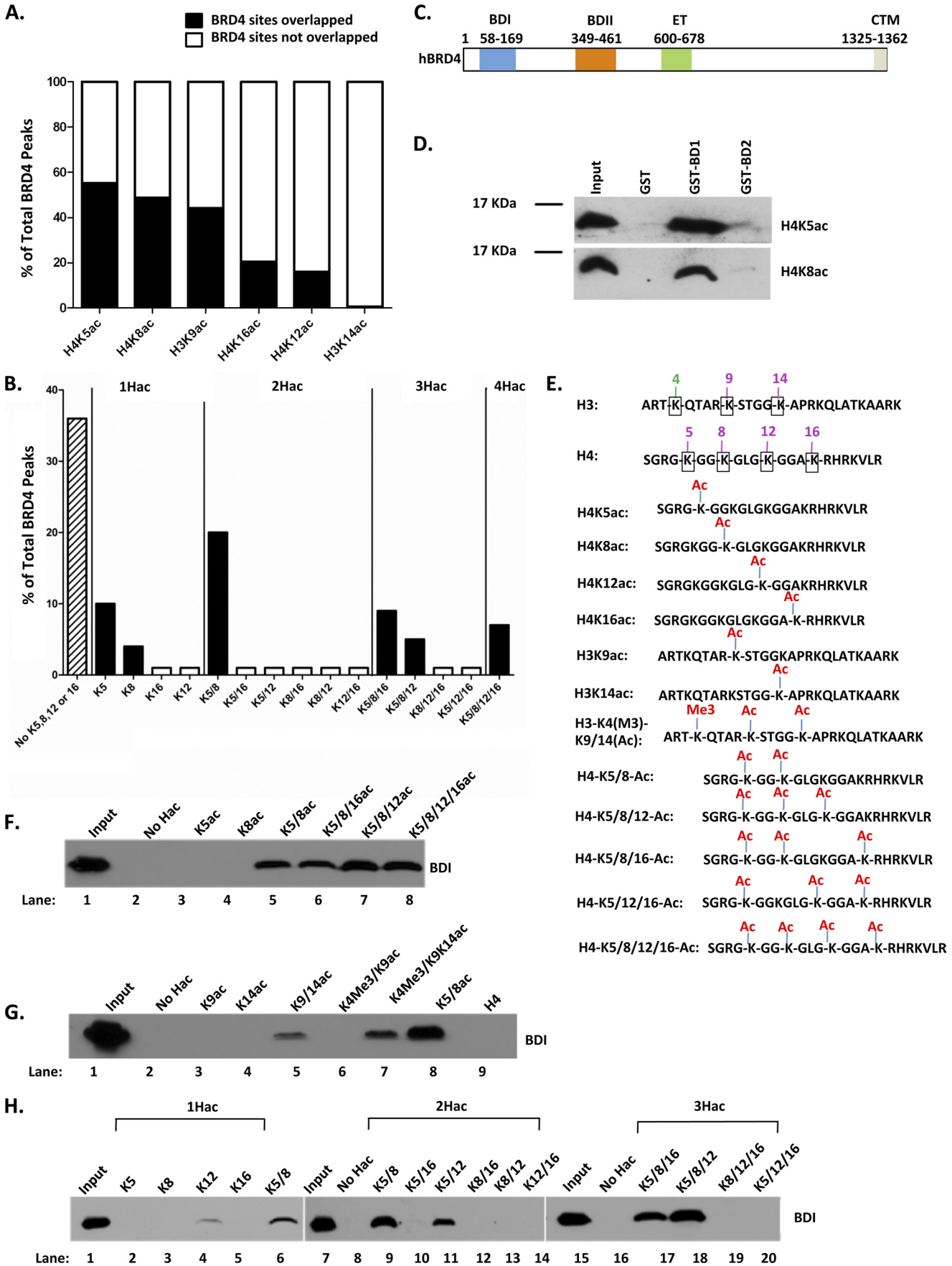
A.
BRD4 sites overlapped
BRD4 sites not overlapped
% of Total BRD4 Peaks
H4K5ac
H4K8ac
H3K9ac
H4K16ac
H4K12ac
H3K14ac
C.
BDI
BDII
ET
CTM
1 58-169
349-461
600-678
1325-1362
hBRD4
D.
Input
GST
GST-BD1
GST-BD2
17 KDa
17 KDa
H4K5ac
H4K8ac
B.
1Hac
2Hac
3Hac
4Hac
% of Total BRD4 Peaks
No K5,8,12 or 16
K5
K8
K16
K12
K5/8
K5/16
K5/12
K8/16
K8/12
K12/16
K5/8/16
K5/8/12
K8/12/16
K5/12/16
K5/8/12/16
E.
H3: ART-K-QTAR-K-STGG-K-APRKQLATKAARK
H4: SGRG-K-GG-K-GLG-K-GGA-K-RHRKVLR
H4K5ac: SGRG-K-GGKGLGKGGAKRHRKVLR
H4K8ac: SGRGKGG-K-GLGKGGAKRHRKVLR
H4K12ac: SGRGKGGKGLG-K-GGAKRHRKVLR
H4K16ac: SGRGKGGKGLGKGGA-K-RHRKVLR
H3K9ac: ARTKQTAR-K-STGGKAPRKQLATKAARK
H3K14ac: ARTKQTARKSTGG-K-APRKQLATKAARK
H3-K4(M3)-K9/14(Ac): ART-K-QTAR-K-STGG-K-APRKQLATKAARK
H4-K5/8-Ac: SGRG-K-GG-K-GLGKGGAKRHRKVLR
H4-K5/8/12-Ac: SGRG-K-GG-K-GLG-K-GGAKRHRKVLR
H4-K5/8/16-Ac: SGRG-K-GG-K-GLGKGGA-K-RHRKVLR
H4-K5/12/16-Ac: SGRG-K-GGKGLG-K-GGA-K-RHRKVLR
H4-K5/8/12/16-Ac: SGRG-K-GG-K-GLG-K-GGA-K-RHRKVLR
F.
Input
No Hac
K5ac
K8ac
K5/8ac
K5/8/16ac
K5/8/12ac
K5/8/12/16ac
BDI
Lane: 1 2 3 4 5 6 7 8
G.
Input
No Hac
K9ac
K14ac
K9/14ac
K4Me3/K9ac
K4Me3/K9K14ac
K5/8ac
H4
BDI
Lane: 1 2 3 4 5 6 7 8 9
H.
1Hac
2Hac
3Hac
Input
K5
K8
K12
K16
K5/8
Input
No Hac
K5/8
K5/16
K5/12
K8/16
K8/12
K12/16
Input
No Hac
K5/8/16
K5/8/12
K8/12/16
K5/12/16
BDI
Lane: 1 2 3 4 5 6 7 8 9 10 11 12 13 14 15 16 17 18 19 20

with additional acetylations, was the only histone configuration that demonstrated global enrichment at BRD4 binding sites as well as positive peptide binding.

HATs and HDACs Are Associated with BRD4 Binding Sites Enriched in H4 Acetylation—Histone acetylations at lysine residues are co-regulated by HATs and HDACs, with the resultant histone acetylation patterns being determined by the antagonistic interplay between these two classes of enzyme (20). To gain mechanistic insight into how acetylation patterns at BRD4 binding sites are established in human CD4+ T cells, we systematically quantified the presence of HATS and HDACs at BRD4 binding sites that displayed at least one of four predominant H4 acetylations (H4K5, H4K8, H4K12, and H4K16; $H4ac^+$ hereafter) for comparison with regions that completely lacked these acetylations ($H4ac^-$). By using ChIP-seq data sets obtained from Wang *et al.* (20), we were able to determine that both HATs (p300/CBP-associated factor, CBP, p300, Tip60, and males-absent-on-the-first) and HDACs (HDAC1, HDAC2, HDAC3, and HDAC6) were frequently co-localized at BRD4 binding sites (Fig. 5, *A* and *B*, respectively). Interestingly, all five representative HATs were enriched at $H4ac^+$ sites (21,380 total) but were significantly depleted at $H4ac^-$ sites (12,164 total; Fig. 5*C*). Comparable enrichment was also observed for all four HDACs analyzed (Fig. 5*D*). In addition, levels of Pol II Ser-2 were far higher at $H4ac^+$ BRD4 binding sites than those detected at $H4ac^-$ BRD4 sites (Fig. 5*E*). Our results suggest that HATs and HDACs may function collaboratively or sequentially to configure acetylation patterns at enhancers and/or promoters that regulate BRD4 recruitment and thus Pol II phosphorylation at Ser-2.

H3K27ac Distinguishes Two Functionally Distinct Classes of BRD4 Binding Site—H3K27ac was recently reported to distinguish active from inactive enhancers in embryonic stem cells and in several adult cell lineages in the mouse (34, 35). Our analyses in human CD4+ T cells revealed that mark H3K27ac was enriched at BRD4-bound sites that exhibited $H4ac^+$ patterns (Fig. 5*F*). To determine whether the presence of H3K27ac at BRD4-bound sites correlated with the activity of nearby genes, we integrated ChIP-seq data sets for BRD4, H3K27ac, and DHS (22) with RNA-seq gene expression data in human CD4+ T cells. Genes with BRD4/H3K27ac overlapping sites displayed significantly higher levels of gene expression than genes that displayed BRD4 binding alone (Fig. 5*G*). Because BRD4 binding sites that lacked H3K27ac coincided with $H4ac^-$ sites, the differences in gene expression observed here are consistent with the HAT, HDAC, and Pol II Ser-2 enrichment previously identified at $H4ac^+$ BRD4 binding sites. Crucially, genes that displayed BRD4/H3K27ac overlapping sites displayed significantly higher gene expression than H3K27ac sites that lacked BRD4 binding, clearly reflecting a contribution of BRD4 to the activity of H3K27ac-enriched enhancers.

BRD4 Regulates Pol II Ser-2 Phosphorylation—JQ1 is a small molecule inhibitor that blocks the binding of bromodomain and extraterminal domain nuclear proteins (BETs) to acetylated histones (36). A previous study in murine bone marrow-derived macrophages demonstrated that BETs primarily affect the expression of inducible genes but exert little effect on the expression of constitutively expressed genes (37). We therefore investigated whether disrupting BETs by JQ1 treatment altered the transcription of BRD4-bound, constitutively expressed genes in human CD4+ T cells. When assessed by quantitative PCR, expression of a representative subset of BRD4-bound genes associated with archetypal T cell functions (*CXCR4*, *RUNX3*, *CD4*, *IL2RA*, and *FOS*) was significantly reduced by JQ1 treatment (Fig. 6*A*). These data indicated that BET proteins, including BRD4, may positively regulate the expression of constitutively expressed lineage-specific genes in primary human CD4+ T cells.

We next used RNA-seq analysis to examine gene expression profiles in primary human CD4+ T cells treated or not with JQ1. Using this approach, we identified 1055 highly expressed BRD4-bound genes (≥5 RPKM) that were substantially down-regulated upon JQ1 treatment (expression reduced by half or more) (supplemental Table S3). These JQ1-sensitive genes included *CXCR4*, *RUNX3*, *CD4*, *IL2RA*, and *FOS*, consistent with our previous quantitative PCR analyses of expression levels of the individual genes in the presence or absence of JQ1 (Fig. 6*A*). We then probed for biological canonical pathways among the 1055 JQ1-sensitive genes by using ingenuity pathways analysis. BRD4 target genes were strongly associated with T cell-specific pathways, including T cell receptor signaling ($p = 1 \times 10^{-6.64}$) (Fig. 6*B*). These data were in-line with the known participation of BRD4 target genes at multiple levels in this pathway, including expression of cell surface molecules (*CD4* and *CD3ϵ*), signaling components (*ZAP70*), and transcriptional regulators (*JUN* and *FOS*). Together, these data demonstrated that JQ1 treatment exerts highly selective effects on expression of BRD4-bound lineage-specific genes in human CD4+ T cells.

A potential mechanism of action for JQ1 was inhibition of Pol II phosphorylation at Ser-2 by disruption of BRD4 binding, leading to decreased gene expression. It could be predicted therefore that JQ1 treatment might decrease BRD4 binding to chromatin, resulting in decreased levels of Ser-2-phosphorylated Pol II. We tested this hypothesis by using ChIP-seq in primary human CD4+ T cells to determine how JQ1 treatment affected BRD4 and Pol II occupancy of binding sites. To achieve this, primary human CD4+ T cells from each donor were pre-

FIGURE 4. **Global association of BRD4 with H4 diacetylation at K5 and K8.** *A*, proportion of total BRD4 binding sites that exhibited specific acetylations within 1 kb of the BRD4 peak max position (*left* to *right*; H4K5ac, H4K8ac, H3K9ac, H4K16ac, H4K12ac, and H3K14ac). *B*, the proportion of BRD4 binding sites associated with different combinatorial patterns of histone acetylations. Percentage of sites with none of the predominant H4 acetylations (*striped bar*) and sites that exhibited H4K5 and H4K8 monoacetylation or combinations of H4K5 and H4K8 acetylation (*black bars*). *C*, representation of BRD4 indicating BD1, BD2, ET, and CTM domains. *D*, Western blot identifying H4K5ac and H4K8ac in mononucleosomes from Jurkat T cells incubated with purified GST, GST-BD1-BRD4, and GST-BD2-BRD4 proteins to demonstrate preferential mononucleosome association with BD1. *E*, positions of lysines that can be acetylated in H3 (first peptide sequence) and H4 (second peptide sequence), and acetylated/trimethylated H4 and H3 synthetic peptides as used for the BD1-peptide binding assays. *F–H*, peptide binding was performed by incubating GST-purified BD1-BRD4 proteins with N terminus-biotinylated synthetic H4 peptides (*F*), various combinations of H3 acetylations (*G*), and H3K4 trimethylation (*H*), and H4 peptides carrying acetylation modifications at specific lysine residues corresponding to *B*. Control peptides used were histones with no modifications. *BDI*, bromodomain I; *BDII*, bromodomain II; *ET*, extraterminal; *CTM*, C-terminal motif.

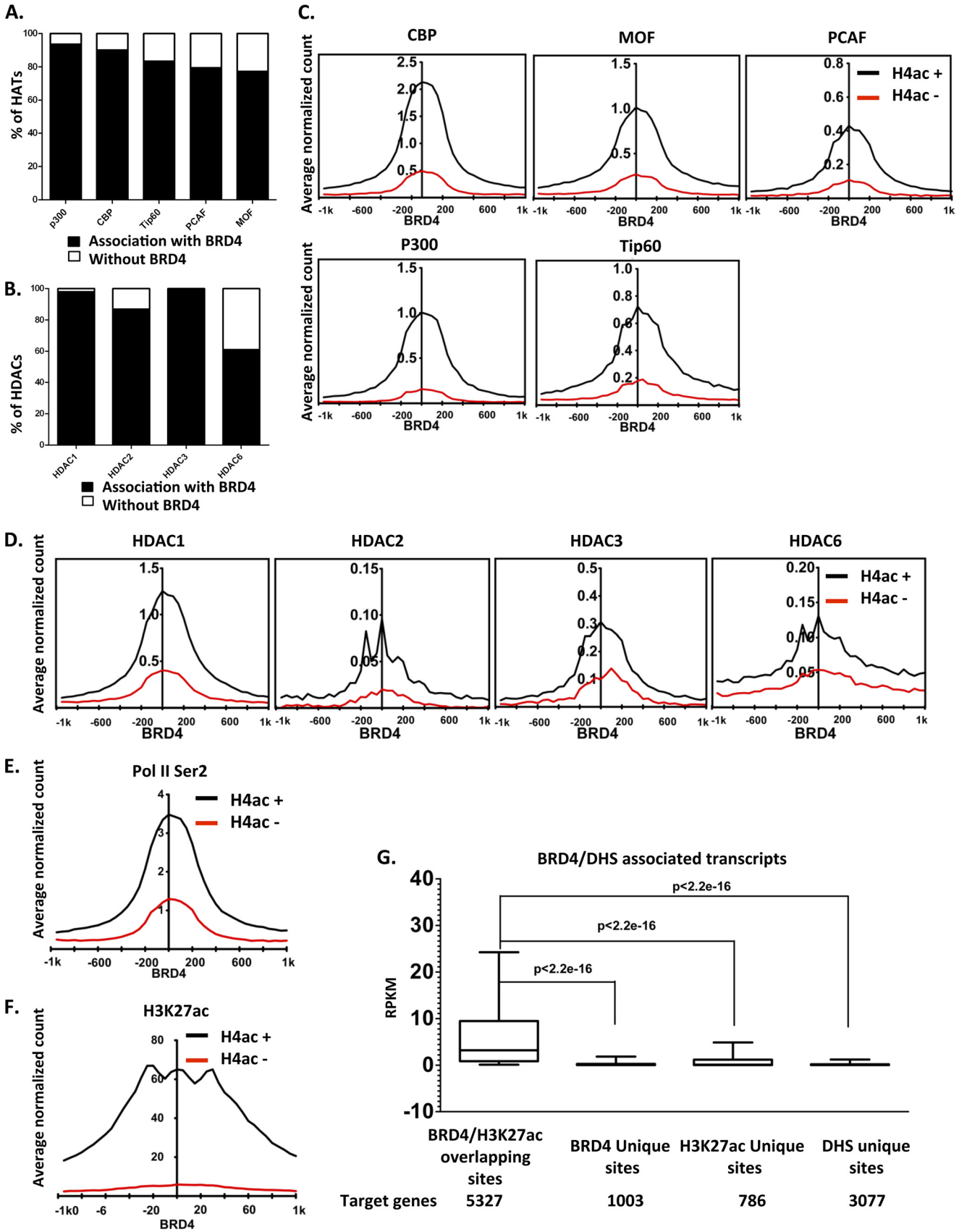
A.
% of HATs
p300
CBP
Tip60
PCAF
MOF
Association with BRD4
Without BRD4
B.
% of HDACs
HDAC1
HDAC2
HDAC3
HDAC6
Association with BRD4
Without BRD4
C.
CBP
MOF
PCAF
P300
Tip60
Average normalized count
BRD4
H4ac +
H4ac -
D.
HDAC1
HDAC2
HDAC3
HDAC6
E.
Pol II Ser2
F.
H3K27ac
G.
BRD4/DHS associated transcripts
RPKM
p<2.2e-16
p<2.2e-16
p<2.2e-16
BRD4/H3K27ac overlapping sites
BRD4 Unique sites
H3K27ac Unique sites
DHS unique sites
Target genes
5327
1003
786
3077

pared both in the absence and presence of JQ1 before chromatin was fixed, sonicated, and dual-immunoprecipitated using antibodies against BRD4 and Pol II in tandem. These assays revealed that JQ1 treatment of human CD4+ T cells significantly reduced BRD4 and Ser-2 Pol II occupancy of JQ1-sensitive genes (Fig. 6*C*). In contrast to the JQ1-sensitive genes *IL2RA*, *FOSL2*, and *MAL*, BRD4, and Ser-2 Pol II binding in the β-2 microglobulin gene, whose expression was not altered by JQ1, revealed no significant change in occupancy (Fig. 6C). We next carried out a global analysis of JQ1 effects on gene occupancy by BRD4, Ser-2 Pol II (Ab5095), Ser-5 Pol II (Ab5131), and total Pol II (4H8) across BRD4 target genes. As expected, JQ1 disrupted BRD4 binding at promoters and gene bodies in human CD4+ T cells (Fig. 6*D*, *top left*). However, ChIP-seq analysis of Ser-2 Pol II indicated that JQ1-sensitive BRD4 target genes generally retained Ser-2 Pol II levels at promoters and displayed significantly reduced Ser-2 Pol II density across the gene body (Fig. 6*D*, *bottom left*). A similar distribution was also observed by using the 4H8 antibody against total Pol II (38) (Fig. 6*D*, *bottom right*). Interestingly, the distribution of Ser-5 Pol II in both promoter regions and gene bodies was largely unaffected by JQ1 exposure (Fig. 6*D*, *top right*). JQ1 treatment also reduced BRD4, Ser-2 Pol II, and total Pol II (4H8) occupancy of intergenic and intragenic regions but exerted little effect on the levels of Ser-5 Pol II present at intergenic and intragenic enhancers (Fig. 6*E*). These observations are consistent with the concept that BRD4 plays a key role in Pol II elongation at target genes in primary human CD4+ T cells by inducing Ser-2 phosphorylation of Pol II.

Lineage-specific BRD4 Binding in Human CD4+ T Cells and Embryonic Stem Cells—BRD4 binding at enhancers and promoters was associated with lineage-specific genes in human CD4+ T cells (*CD4* and *LCK*), so we next investigated whether BRD4 was associated with cell type-specific programs of transcription. We performed ChIP-seq in hESCs to identify a total of 33,988 BRD4 binding sites across the genome. Approximately 50% of the BRD4 binding sites shared genetic loci in both hESCs and in T cells (15,411 BRD4 peaks in T cells had a hESC BRD4 peak within 2.5 kb of their peak max position), whereas the remaining 50% of BRD4 binding sites displayed a differential distribution between cell types (Fig. 7*A*). Although a large fraction of BRD4 binding sites in promoters were shared between cell types (Fig. 7*B*), the enhancer sites were largely distinct (Fig. 7*C*), indicating that enhancer elements may influence the lineage-specific binding of BRD4. Lineage-specific BRD4 binding in T cells occurred in genes that regulate T cell-specific functions, including T cell receptor signaling (Fig. 7*D*), whereas binding in hESC occurred in genes that maintain pluripotency (Fig. 7*E*). Genes that displayed BRD4 binding sites in both hESC and T cell lineages were instead involved in general cell metabolism (Fig. 7*F*). These data indicate that BRD4 may play an important role in lineage-specific gene expression programs and that BRD4 regulates Pol II Ser2 phosphorylation to influence gene transcription in hESCs as well as in human CD4+ T cells.

We next mapped BRD4 binding sites and DHS in human CD4+ T cells to establish the efficacy of this approach for mapping regulatory elements across the genome. The DHS data set identifying active genes in human CD4+ T cell was adapted from a published study (22). In terms of target genes, the distribution of BRD4 binding sites and DHS were remarkably similar in our analyses (Fig. 7*G*). These data demonstrated that BRD4 could potentially be used as a genome-wide hallmark of active or poised genes in CD4+ T cells. An examination of BRD4 binding sites and DHS at promoters (sites within 2 kb of a Refseq TSS) indicated that 96% of BRD4 binding sites at promoters were associated with a DHS, whereas 74% of promoter DHS also displayed a BRD4 binding site (Fig. 7*H*). These analyses indicated that both BRD4 binding and DNase I assays can identify promoters in the genome of human CD4+ T cells. We next assessed the efficiency with which transcriptional enhancers were identified by BRD4 binding when compared with DNase1 assays. Enhancer binding sites were defined as gene-associated sites at least a 2-kb distance from a TSS. Surprisingly, many enhancer sites were detected by only one of the two assays; 55% of enhancer BRD4 binding sites exhibited a DHS within 1 kb of their peak max position, whereas only 40% of DHS incorporated a BRD4 binding site within 1 kb of their peak max (Fig. 7*I*). These data suggest that the broadest identification of enhancer regulatory elements across the genome may require analyses of both BRD4 binding and DHS distribution.

BRD4 Regulation of Pol II Ser-2 Phosphorylation via P-TEFb at a Subset of Enhancers—We used ChIP-seq to determine BRD4 and Pol II Ser-2 occupancy of promoters and enhancers across the genome in primary human CD4+ T cells. Our data revealed that average BRD4 and Pol II Ser-2 peak max position are in close proximity at promoters (Fig. 8*A*, *left panel*) and enhancer binding sites (Fig. 8*A*, *right panel*), thus suggesting that BRD4 can regulate Pol II Ser-2 phosphorylation via effects on P-TEFb, which is known to form a complex with BRD4. Immunoprecipitation of CDK9 (a subunit of the P-TEFb complex) in Jurkat human T cells confirmed an interaction with BRD4, and BRD4 immunoprecipitated with CDK9, further verifying the association between these molecules (Fig. 8*B*). These data are also consistent with reports from other investigators that CDK9 interacts with BRD4 in HeLa cells (10, 26). Accordingly, we were able to detect binding of P-TEFb at sites where BRD4 and Pol II co-localized. In addition, ChIP analyses of BRD4-bound and Pol II Ser-2-bound regions indicated that CDK9 binding capacity was increased at multiple BRD4 and

FIGURE 5. **Two distinct classes of BRD4 binding confer different levels of gene transcription.** Percentage of total HATs (*A*; p300, CBP, Tip60, p300/CBP-associated factor, males-absent-on-the-first) and HDACs (*B*; HDAC1, HDAC2, HDAC3, and HDAC6) that displayed BRD4 binding within 1 kb of the enzyme peak max position. *C–F*, average normalized tag count distribution in 2-kb windows centered on untreated BRD4 binding peak max positions for two classes of BRD4 binding sites: H4ac$^+$ sites (one or more H4 acetylations; *black*) and H4ac$^-$ sites (no H4 acetylations; *red*) for HATs (*C*), HDACs (*D*), Pol II Ser-2 (*E*), and H3K27ac (*F*). *G*, box plots showing the 10–90th percentile of the RNA-seq RPKM expression range for genes with BRD4 and H3K27ac overlapping sites, BRD4 unique sites (genes displaying BRD4 binding but not H3K27ac), H3K27ac unique sites (genes displaying H3K27ac but not BRD4 binding) and DHS unique sites (genes displaying DHS but not H3K27ac or BRD4). Non-parametric analysis of variance (Kruskal-Wallis test) p value $<2.2 \times 10^{-16}$. Pairwise Wilcoxon rank-sum test p values (Bonferroni-adjusted) are indicated in the figure.

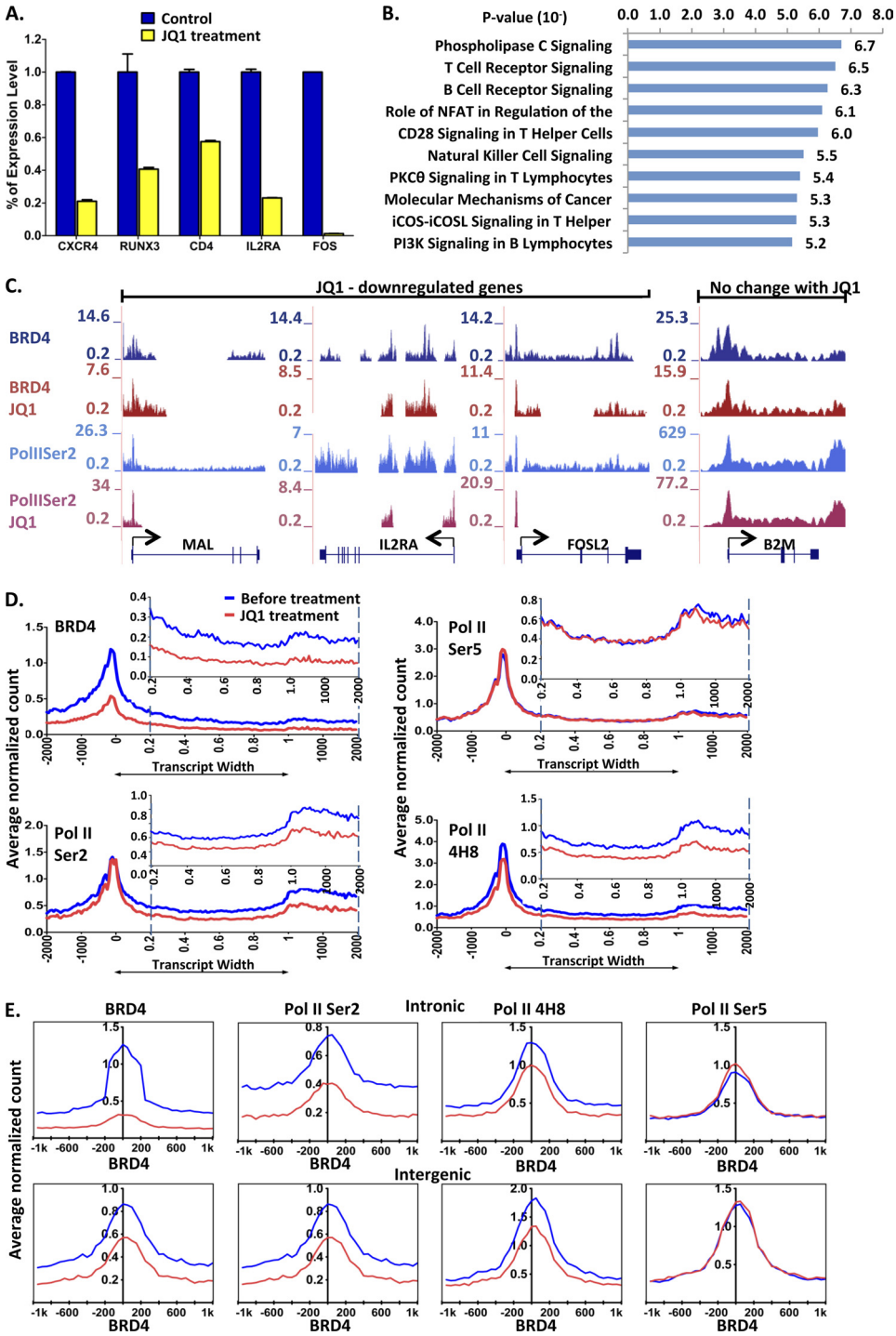

FIGURE 6. **BRD4 regulates Pol II phosphorylation at Ser-2.** *A,* RNA expression of *CXCR4*, *RUNX3*, *CD4*, *IL2RA* and *FOS* in untreated CD4+ T cells (*blue bars*) and JQ1-treated CD4+ T cells (*yellow bars*) expressed as a ratio of the mean gene expression in the untreated cells (error bars indicate S.D. of at least three independent sets of experimental data). *B*, top 10 enriched pathways identified by Ingenuity Pathway Analysis for JQ1-sensitive BRD4 target genes, ordered by decreasing negative log10 *p* values. *C*, UCSC genome browser view of normalized BRD4 and Pol II Ser-2 binding at JQ1-sensitive genes *MAL*, *IL2RA,* and *FOSL2* (*left* to *right*) compared with JQ1-resistant gene *B2M* both pre- (*blue tracks*) and post- (*red tracks*) JQ1 treatment. *D*, average normalized tag count distribution in the 2 kb upstream region, 2kb downstream region, and in the gene body for all JQ1-sensitive BRD4-associated refseq transcripts. Distributions shown are BRD4 (*top left*), Pol II Ser-2 (*bottom left*), Pol II Ser-5 (*top right*), and total Pol II (4H8) (*bottom right*) both before (*blue* profile) and after JQ1 treatment (*red* profile). '0' - TSS and '1' - transcription termination site (TTS). *E*, average normalized tag count distribution in 2-kb windows centered on enhancer BRD4 peak max positions for BRD4 (*left panel*), Pol II Ser-2 (*middle left panel*), total Pol II (4H8) (*middle left panel*), and Pol II Ser-5 (*right panel*). Tag count distributions were plotted for intronic enhancers (*top panel*) and intergenic enhancers (*bottom panel*). Profile coloration is consistent with *D*.

Pol II Ser-2 co-localization sites in both promoter and enhancer regions of the genes *CXCR4* (Fig. 8*C*), *FOS* (Fig. 8*D*), and *CXCR5* (Fig. 8*E*). These data support our conclusion that, at least for a subset of enhancers, co-localization with Pol II may promote BRD4 regulation of Pol II Ser-2 phosphorylation via effects on P-TEFb. Whether this observation can also be extended to other enhancers remains unclear. Alternatively, BRD4 may act as an atypical kinase

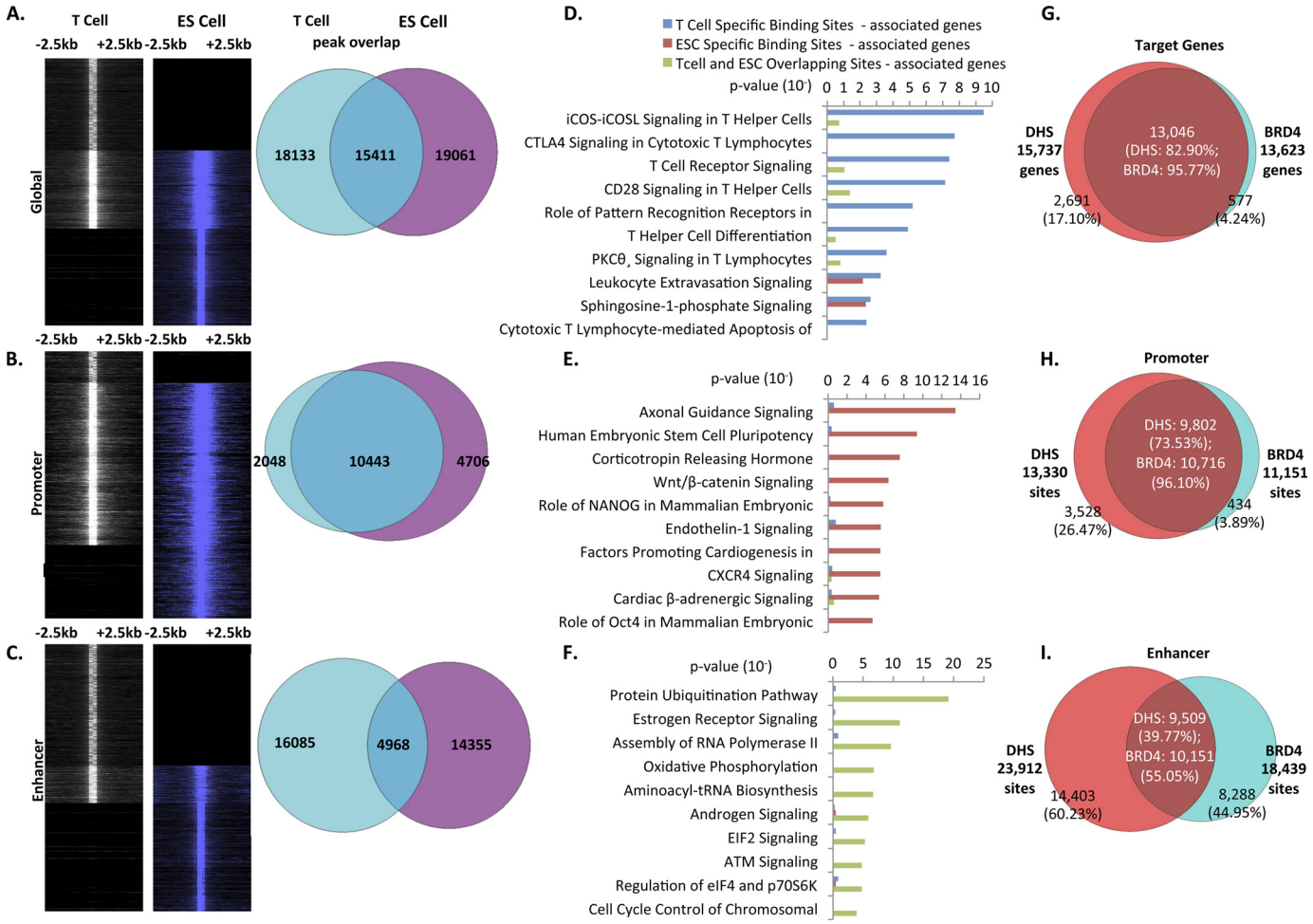

FIGURE 7. **Lineage-specific BRD4 binding in CD4+ T cells and hESCs.** *A*, *left*: heat map illustrating normalized tag counts for BRD4 in T cells (*white*) and hESCs (*purple*) in 5-kb windows centered on BRD4 peak max (33,544 loci in T cells, 19,061 loci in hESC). *Right*: Venn diagram representation of global peak overlap between 5-kb windows centered on T cell peak max positions (*teal*) and hESC peaks (*purple*). *B*, *left*: heat map illustrating normalized tag counts for BRD4 in T cells (*white*) and hESCs (*purple*) in 5-kb windows centered on BRD4 peak max at promoters (12,491 loci in T cells, and 4,706 loci in hESC). *Right*: Venn diagram representation of peak overlap between 5-kb windows centered on T cell promoter peak max positions (*teal*) and hESC peaks (*purple*). *C*, *left*: heat map illustrating normalized tag counts for BRD4 in T cells (*white*) and hESCs (*purple*) in 5-kb windows centered on enhancer peak max (21,053 loci in T cells; 14,355 loci in hESCs). *Right*: Venn diagram representation of peak overlap between 5-kb windows centered on T cell enhancer peak max positions (*teal*) and hESC peaks (*purple*). *D*, selected ingenuity pathway analysis pathways and negative log10 *p* values for gene sets categorized according to the presence of T cell-specific sites (*blue*), hESC-specific sites (*red*), and T cell and hESC overlapping sites (*green*). *Top*, T cell-related pathways; *middle*, ESC-related pathways; and *bottom*, general cell function pathways. *G–I*, Venn diagram representation of CD4+ T cells showing target gene overlap between DHS-associated genes (*red*) and BRD4-associated genes (*teal*; *G*); promoter peak overlap between DHS (*red*) and BRD4 peaks (*teal*) at the promoter (*H*); enhancer peak overlap between DHS (*red*) and BRD4 peaks (*teal*) at enhancer regions (*I*). Value *under* library label indicates the total number of DHS/BRD4 sites used in each comparison. *White text*, number/percentage of overlapping genes/sites in each library. *Black text* on Venn diagram indicates number/percentage of non-overlapping genes/sites in each library.

that directly promotes Ser-2 phosphorylation of Pol II independently of P-TEFb (39).

DISCUSSION

Using genome-wide analyses, we observed that BRD4 is recruited to the majority of active genes in primary human CD4+ T cells. A role for BRD4 in P-TEFb recruitment was previously known only for stimulus-specific genes, such as Toll-like receptor-inducible genes in murine bone marrow-derived macrophages (8). Similarly, alternative P-TEFb-tethering transcription factors such as NF-κB and class II, major histocompatibility complex, transactivator have been shown to regulate only a subset of inducible genes (40, 41). However, our findings demonstrate that BRD4 regulation of Pol II Ser-2 phosphorylation is not restricted to inducible genes but extends to constitutively active genes in human CD4+ T cells. Nearly all of the Pol II Ser-2-bound promoters exhibited BRD4 co-binding, and numerous enhancers were associated with tandem binding of BRD4 and Pol II Ser-2, including several regions in the *IL2RA* gene and well defined enhancer elements in the *CD4* gene. Global analyses confirmed that Pol II occupancy of enhancers is closely correlated with the enrichment of H3K4me3 and H3K9ac at distal regulatory elements. However, we were unable to detect any interaction between BRD4 and Pol II when using co-immunoprecipitation approaches in Jurkat human T cells (data not shown). Treatment of human CD4+ T cells with inhibitor JQ1 reduced BRD4 binding and consequently decreased Pol II Ser-2 levels at enhancers and gene bodies in a subset of T cell-associated genes. Taken together, these findings suggest that phosphorylation of Pol II at Ser-2 in human

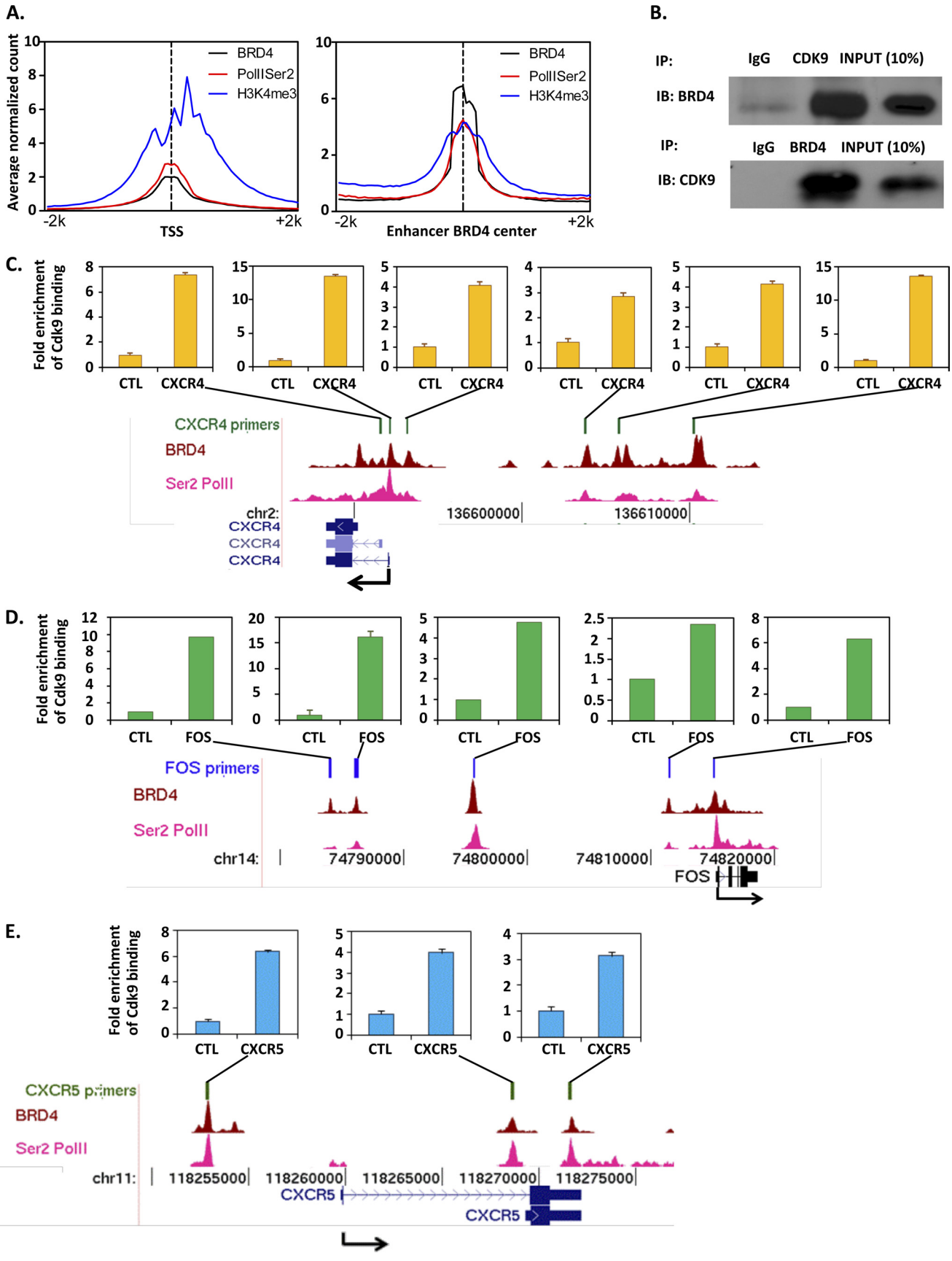
A.
Average normalized count
BRD4
PolIISer2
H3K4me3
-2k
TSS
+2k
Enhancer BRD4 center
B.
IP:
IgG
CDK9
INPUT (10%)
IB: BRD4
IP:
IgG
BRD4
INPUT (10%)
IB: CDK9
C.
Fold enrichment of Cdk9 binding
CTL
CXCR4
CXCR4 primers
BRD4
Ser2 PolII
chr2:
136600000
136610000
CXCR4
CXCR4
CXCR4
D.
Fold enrichment of Cdk9 binding
CTL
FOS
FOS primers
BRD4
Ser2 PolII
chr14:
74790000
74800000
74810000
74820000
FOS
E.
Fold enrichment of Cdk9 binding
CTL
CXCR5
CXCR5 primers
BRD4
Ser2 PolII
chr11:
118255000
118260000
118265000
118270000
118275000
CXCR5
CXCR5

CD4+ T cells depends on Pol II co-localization with BRD4, which perhaps mediates the recruitment of P-TEFb.

The relationship between Pol II Ser-2 and BRD4 in regulating transcription has been demonstrated primarily for promoters (8, 26). However, it has also been reported that the BRD4-CDK9 complex can bind to the FOSL1 gene enhancer (9) and to the IgH enhancer in MM.1S cells (30). Our genome-wide analysis revealed that BRD4 and Pol II Ser-2 do indeed both bind to putative enhancers in primary human CD4+ T cells. By observing that a number of genes displayed binding of BRD4 or Pol II Ser-2 at putative enhancers but not at promoters (supplemental Fig, S3*f*), we also demonstrated that at least one mechanism of recruitment involves BRD4/Pol II Ser2 binding independently of the promoter. It has been proposed that recruitment of the preinitiation complex to enhancers allows genes to be maintained in a potentiated state that regulates the timing of gene transcription (14). It is possible that BRD4 and Pol II Ser2 binding at enhancers form part of this regulatory apparatus.

We observed that BRD4 disruption by JQ1 treatment in primary human CD4+ T cells substantially reduced the levels of BRD4 binding at promoters but did not affect the levels of Ser-2 phosphorylated Pol II located near the TSS of target genes. This finding implies that a mechanism distinct from BRD4-Pol II Ser-2 interaction may occur in the promoter regions of genes expressed in primary human CD4+ T cells. A possible BRD4-independent mechanism of P-TEFb recruitment could be via PAF1- and/or Med26-mediated sequestration of the super elongation complex, which incorporates P-TEFb (42). Intriguingly, the amount of Ser-2 Pol II we detected throughout the coding regions of genes was found to be significantly reduced after JQ1 treatment, which mirrored the decrease in BRD4 binding in the coding regions of genes after JQ1 exposure. These findings suggested that the initial Ser-2 phosphorylation of Pol II is mediated by a BRD4-independent mechanism, whereas sustained Ser-2 phosphorylaton of Pol II is mediated by BRD4 during the transition from transcription initiation to elongation.

Genome-wide studies have established that distal regulatory regions including enhancers are generally characterized by H3K4me1 (43), whereas H3K4me3 is a hallmark of gene promoters. Our detection of H3K4me3 enrichment and Pol II binding at a significant fraction of enhancers in primary human CD4+ T cells could potentially have arisen from misidentification of unannotated promoters as enhancers. However, several lines of evidence suggest that the distal regulatory regions we identified in human CD4+ T cells are genuine enhancer elements. First, unlike promoters, intergenic and intragenic enhancers are generally not associated with CpG islands; we rarely detected CpG islands in the regions identified as intergenic enhancers (21%) or intragenic enhancers (8%), whereas CpG islands were detected in the majority (85%) of BRD4-bound promoters. Second, promoters have been shown to exhibit high levels of H3K4me, whereas the level of H3K4me3 we detected at intergenic and intragenic enhancers was significantly lower than that observed at promoters. Thirdly, we detected H3K4me3 and Pol II at well characterized enhancer elements in T cell-specific genes, including *CD4* and *IL2RA*. Lastly, the H3K4me3-enriched intergenic and intragenic enhancers were found to be significantly associated with the presence of H3K27ac, which was recently reported to characterize developmentally active enhancers in a number of different cell types, including murine embryonic stem cells and pro-B cells. Our finding is also consistent with a recent study that reported the detection of H3K4me3 at the enhancers of T cell-specific genes in developing murine thymocytes (31). Moreover, the authors showed that the induction of H3K4me3 at T cell-specific gene enhancers is strongly correlated with the functional activity of these enhancers during differentiation. Together, these studies in both mouse and human T cells suggest that the presence of H3K4me3 at enhancers may be more common than previously thought and could serve an important role in enhancer activation during T cell development.

To identify possible determinants of genome-wide BRD4 recruitment, we probed for a histone acetylation pattern that demonstrated genome-wide co-localization with BRD4 binding sites and exhibited interaction with BRD4 supported by positive acetylated histone peptide binding with the BD1 bromodomain. BRD4 binding sites were enriched in H4K5 and H4K8 monoacetylation or in multiacetylated H4 patterns that included H4K5ac and H4K8ac. Histone acetylation peptides that exhibited both H4K5ac and H4K8ac displayed positive BD1 binding, but monoacetylations that were observed to be associated with BRD4 binding sites *in vivo* could not support binding *in vitro*. An additional histone acetylation other than the four variants analyzed here might therefore contribute to BRD4 binding at H4K5 and H4K8 monoacetylation sites. Other peptides that displayed positive BD1 binding were H4K5/12ac and H3K9/14ac, but neither variant was globally enriched at BRD4 binding sites. Thus, H4K5/8ac, either alone or in combination with additional acetylations, was the only histone acetylation pattern that was both enriched at BRD4 binding sites and displayed positive peptide binding.

We found that H3K27ac was enriched at histone acetylation-associated BRD4 binding sites ($H4ac^+$). However, BRD4 failed to bind to synthetic H3K27ac peptides (data not shown). H3K27ac has recently been shown to distinguish active enhancers (34, 35), and we observed that H3K27ac sites with associated BRD4 and Pol II Ser-2 binding were accompanied by higher gene activity than sites exhibiting H3K27ac alone, suggesting that BRD4 contributes to the activity of H3K27ac-enriched regions. The presence of HATs, HDACs, H3K27ac, H3K4me3, H3K9ac, and Pol II Ser-2 along with BRD4 was specific to $H4ac^+$ BRD4 binding sites. Genes associated with these $H4ac^+$ binding sites also displayed significantly higher gene expression levels. A number of different transcription factors interact with HATs and HDACs (44) and could potentially configure a chro-

FIGURE 8. **BRD4 regulates Pol II Ser-2 phosphorylation via P-TEFb.** *A*, average normalized tag count distribution in 4-kb windows centered on the TSS (*left panel*) and enhancer BRD4 peak max (*right panel*) for BRD4, Pol II Ser-2, and H3K4me3. *B*, co-immunoprecipitation of BRD4 and CDK9 using antibodies against IgG, CDK9, and BRD4. Immunoprecipitated proteins were analyzed by Western blotting with anti-BRD4 (*top panel*) or anti-CDK9 (*bottom panel*). *C–E*, ChIP of CDK9 at regions where both BRD4 and Pol II Ser-2 binding were observed in Jurkat T cells; *CXCR4* (*C*), *FOS* (*D*), and *CXCR5* (*E*). Primer sites are shown on the figure.

matin environment conducive to BRD4 binding and P-TEFb recruitment. We have identified that H4K5ac and H4K8ac permit BRD4 recruitment, whereas H3K9ac and H3K4me3 may provide a platform for Pol II binding. This combination of histone modifications allows BRD4 and Pol II to co-localize at both promoters and enhancer elements.

The mechanism we propose for the involvement of BRD4 in regulating Ser-2 Pol II has wide-reaching implications for the regulation of gene transcription across many different cell types. In the current report, BRD4 binding in hESCs was as frequent as that observed in human primary CD4+ T cells, with approximately half of the binding sites identified occurring at common genetic loci. Lineage-specific BRD4 binding sites were associated with cell type-specific genes, whereas genes with BRD4 binding sites shared between cell types were instead associated with general metabolic activities. Binding sites shared between the two lineages were found mainly at promoters, whereas enhancer binding sites were largely exclusive to each lineage, indicating that BRD4 binding at enhancers is more variable than at promoters. BRD4 is both broadly expressed and highly conserved across multiple cell types in diverse organisms, such that genome-wide identification of BRD4 binding could represent a novel means of identifying active promoters and lineage-specific enhancer elements in many different cell populations.

The ability of JQ1 to inhibit a subset of T cell-associated genes in human CD4+ T cells may pave the way for the therapeutic targeting of BETs, including BRD4, in the treatment of T cell-mediated diseases. The continuing development of increasingly specific pharmacological inhibitors of different nuclear proteins in the BET family will facilitate a better understanding of how these proteins contribute to transcription regulation in different subsets of human CD4+ T cells. This may eventually lead to the identification of novel strategies for intervening in human inflammatory disorders that are characterized by specific programs of T cell differentiation.

Acknowledgments—We thank Dr. Lucy Robinson and Dr. Neil McCarthy of Insight Editing London and Dr. Michael Poidinger for critical review and help in manuscript preparation and Dr. Francesca Zolezzi and Josephine Lum from SIgN Functional Genomics core for sequencing data generation. We thank Dr. Ng Huck Hui for providing hESC-derived chromatin and thank Drs. Li Guoliang and Sung Wing-Kin Ken for the script needed to perform tag count distributions. We are grateful to Mickey B. C. Koh and the Health Sciences Authority of Singapore for providing healthy human blood for use in this study.

REFERENCES

1. Hochheimer, A., and Tjian, R. (2003) Diversified transcription initiation complexes expand promoter selectivity and tissue-specific gene expression. *Genes Dev.* **17,** 1309–1320
2. Rahl, P. B., Lin, C. Y., Seila, A. C., Flynn, R. A., McCuine, S., Burge, C. B., Sharp, P. A., and Young, R. A. (2010) c-Myc regulates transcriptional pause release. *Cell* **141,** 432–445
3. Guenther, M. G., Levine, S. S., Boyer, L. A., Jaenisch, R., and Young, R. A. (2007) A chromatin landmark and transcription initiation at most promoters in human cells. *Cell* **130,** 77–88
4. Kim, T. H., Barrera, L. O., Zheng, M., Qu, C., Singer, M. A., Richmond, T. A., Wu, Y., Green, R. D., and Ren, B. (2005) A high-resolution map of active promoters in the human genome. *Nature* **436,** 876–880
5. Hirose, Y., and Ohkuma, Y. (2007) Phosphorylation of the C-terminal domain of RNA polymerase II plays central roles in the integrated events of eucaryotic gene expression. *J. Biochem.* **141,** 601–608
6. Wu, S. Y., and Chiang, C. M. (2007) The double bromodomain-containing chromatin adaptor Brd4 and transcriptional regulation. *J. Biol. Chem.* **282,** 13141–13145
7. Dey, A., Chitsaz, F., Abbasi, A., Misteli, T., and Ozato, K. (2003) The double bromodomain protein Brd4 binds to acetylated chromatin during interphase and mitosis. *Proc. Natl. Acad. Sci. U.S.A.* **100,** 8758–8763
8. Hargreaves, D. C., Horng, T., and Medzhitov, R. (2009) Control of inducible gene expression by signal-dependent transcriptional elongation. *Cell* **138,** 129–145
9. Zippo, A., Serafini, R., Rocchigiani, M., Pennacchini, S., Krepelova, A., and Oliviero, S. (2009) Histone crosstalk between H3S10ph and H4K16ac generates a histone code that mediates transcription elongation. *Cell* **138,** 1122–1136
10. Jang, M. K., Mochizuki, K., Zhou, M., Jeong, H. S., Brady, J. N., and Ozato, K. (2005) The bromodomain protein Brd4 is a positive regulatory component of P-TEFb and stimulates RNA polymerase II-dependent transcription. *Mol. Cell* **19,** 523–534
11. Johnson, K. D., Christensen, H. M., Zhao, B., and Bresnick, E. H. (2001) Distinct mechanisms control RNA polymerase II recruitment to a tissue-specific locus control region and a downstream promoter. *Mol. Cell* **8,** 465–471
12. Johnson, K. D., Grass, J. A., Park, C., Im, H., Choi, K., and Bresnick, E. H. (2003) Highly restricted localization of RNA polymerase II within a locus control region of a tissue-specific chromatin domain. *Mol. Cell Biol.* **23,** 6484–6493
13. Louie, M. C., Yang, H. Q., Ma, A. H., Xu, W., Zou, J. X., Kung, H. J., and Chen, H. W. (2003) Androgen-induced recruitment of RNA polymerase II to a nuclear receptor-p160 coactivator complex. *Proc. Natl. Acad. Sci. U.S.A.* **100,** 2226–2230
14. Szutorisz, H., Dillon, N., and Tora, L. (2005) The role of enhancers as centres for general transcription factor recruitment. *Trends Biochem. Sci.* **30,** 593–599
15. Kim, T. K., Hemberg, M., Gray, J. M., Costa, A. M., Bear, D. M., Wu, J., Harmin, D. A., Laptewicz, M., Barbara-Haley, K., Kuersten, S., Markenscoff-Papadimitriou, E., Kuhl, D., Bito, H., Worley, P. F., Kreiman, G., and Greenberg, M. E. (2010) Widespread transcription at neuronal activity-regulated enhancers. *Nature* **465,** 182–187
16. Wang, Q., Carroll, J. S., and Brown, M. (2005) Spatial and temporal recruitment of androgen receptor and its coactivators involves chromosomal looping and polymerase tracking. *Mol. Cell* **19,** 631–642
17. Barski, A., Cuddapah, S., Cui, K., Roh, T. Y., Schones, D. E., Wang, Z., Wei, G., Chepelev, I., and Zhao, K. (2007) High-resolution profiling of histone methylations in the human genome. *Cell* **129,** 823–837
18. Barski, A., Chepelev, I., Liko, D., Cuddapah, S., Fleming, A. B., Birch, J., Cui, K., White, R. J., and Zhao, K. (2010) Pol II and its associated epigenetic marks are present at Pol III-transcribed noncoding RNA genes. *Nat. Struct. Mol. Biol.* **17,** 629–634
19. Wang, Z., Zang, C., Rosenfeld, J. A., Schones, D. E., Barski, A., Cuddapah, S., Cui, K., Roh, T. Y., Peng, W., Zhang, M. Q., and Zhao, K. (2008) Combinatorial patterns of histone acetylations and methylations in the human genome. *Nat. Genet.* **40,** 897–903
20. Wang, Z., Zang, C., Cui, K., Schones, D. E., Barski, A., Peng, W., and Zhao, K. (2009) Genome-wide mapping of HATs and HDACs reveals distinct functions in active and inactive genes. *Cell* **138,** 1019–1031
21. Lim, C. A., Yao, F., Wong, J. J., George, J., Xu, H., Chiu, K. P., Sung, W. K., Lipovich, L., Vega, V. B., Chen, J., Shahab, A., Zhao, X. D., Hibberd, M., Wei, C. L., Lim, B., Ng, H. H., Ruan, Y., and Chin, K. C. (2007) Genome-wide mapping of RELA(p65) binding identifies E2F1 as a transcriptional activator recruited by NF-κB upon TLR4 activation. *Mol. Cell* **27,** 622–635
22. Boyle, A. P., Davis, S., Shulha, H. P., Meltzer, P., Margulies, E. H., Weng, Z., Furey, T. S., and Crawford, G. E. (2008) High-resolution mapping and characterization of open chromatin across the genome. *Cell* **132,** 311–322
23. Fejes, A. P., Robertson, G., Bilenky, M., Varhol, R., Bainbridge, M., and

Jones, S. J. (2008) FindPeaks 3.1: a tool for identifying areas of enrichment from massively parallel short-read sequencing technology. *Bioinformatics* **24,** 1729–1730
24. Quinlan, A. R., and Hall, I. M. (2010) BEDTools: a flexible suite of utilities for comparing genomic features. *Bioinformatics* **26,** 841–842
25. Saldanha, A. J. (2004) Java Treeview–extensible visualization of microarray data. *Bioinformatics* **20,** 3246–3248
26. Yang, Z., Yik, J. H., Chen, R., He, N., Jang, M. K., Ozato, K., and Zhou, Q. (2005) Recruitment of P-TEFb for stimulation of transcriptional elongation by the bromodomain protein Brd4. *Mol. Cell* **19,** 535–545
27. Feng, Y., Broder, C. C., Kennedy, P. E., and Berger, E. A. (1996) HIV-1 entry cofactor: functional cDNA cloning of a seven-transmembrane, G protein-coupled receptor. *Science* **272,** 872–877
28. Heintzman, N. D., Stuart, R. K., Hon, G., Fu, Y., Ching, C. W., Hawkins, R. D., Barrera, L. O., Van Calcar, S., Qu, C., Ching, K. A., Wang, W., Weng, Z., Green, R. D., Crawford, G. E., and Ren, B. (2007) Distinct and predictive chromatin signatures of transcriptional promoters and enhancers in the human genome. *Nat. Genet.* **39,** 311–318
29. Roh, T. Y., Cuddapah, S., and Zhao, K. (2005) Active chromatin domains are defined by acetylation islands revealed by genome-wide mapping. *Genes Dev.* **19,** 542–552
30. Delmore, J. E., Issa, G. C., Lemieux, M. E., Rahl, P. B., Shi, J., Jacobs, H. M., Kastritis, E., Gilpatrick, T., Paranal, R. M., Qi, J., Chesi, M., Schinzel, A. C., McKeown, M. R., Heffernan, T. P., Vakoc, C. R., Bergsagel, P. L., Ghobrial, I. M., Richardson, P. G., Young, R. A., Hahn, W. C., Anderson, K. C., Kung, A. L., Bradner, J. E., and Mitsiades, C. S. (2011) BET bromodomain inhibition as a therapeutic strategy to target c-Myc. *Cell* **146,** 904–917
31. Pekowska, A., Benoukraf, T., Zacarias-Cabeza, J., Belhocine, M., Koch, F., Holota, H., Imbert, J., Andrau, J. C., Ferrier, P., and Spicuglia, S. (2011) H3K4 tri-methylation provides an epigenetic signature of active enhancers. *EMBO J.* **30,** 4198–4210
32. Saxonov, S., Berg, P., and Brutlag, D. L. (2006) A genome-wide analysis of CpG dinucleotides in the human genome distinguishes two distinct classes of promoters. *Proc. Natl. Acad. Sci. U.S.A.* **103,** 1412–1417
33. Vermeulen, M., Mulder, K. W., Denissov, S., Pijnappel, W. W., van Schaik, F. M., Varier, R. A., Baltissen, M. P., Stunnenberg, H. G., Mann, M., and Timmers, H. T. (2007) Selective anchoring of TFIID to nucleosomes by trimethylation of histone H3 lysine 4. *Cell* **131,** 58–69
34. Rada-Iglesias, A., Bajpai, R., Swigut, T., Brugmann, S. A., Flynn, R. A., and Wysocka, J. (2011) A unique chromatin signature uncovers early developmental enhancers in humans. *Nature* **470,** 279–283
35. Creyghton, M. P., Cheng, A. W., Welstead, G. G., Kooistra, T., Carey, B. W., Steine, E. J., Hanna, J., Lodato, M. A., Frampton, G. M., Sharp, P. A., Boyer, L. A., Young, R. A., and Jaenisch, R. (2010) Histone H3K27ac separates active from poised enhancers and predicts developmental state. *Proc. Natl. Acad. Sci. U.S.A.* **107,** 21931–21936
36. Filippakopoulos, P., Qi, J., Picaud, S., Shen, Y., Smith, W. B., Fedorov, O., Morse, E. M., Keates, T., Hickman, T. T., Felletar, I., Philpott, M., Munro, S., McKeown, M. R., Wang, Y., Christie, A. L., West, N., Cameron, M. J., Schwartz, B., Heightman, T. D., La Thangue, N., French, C. A., Wiest, O., Kung, A. L., Knapp, S., and Bradner, J. E. (2010) Selective inhibition of BET bromodomains. *Nature* **468,** 1067–1073
37. Nicodeme, E., Jeffrey, K. L., Schaefer, U., Beinke, S., Dewell, S., Chung, C. W., Chandwani, R., Marazzi, I., Wilson, P., Coste, H., White, J., Kirilovsky, J., Rice, C. M., Lora, J. M., Prinjha, R. K., Lee, K., and Tarakhovsky, A. (2010) Suppression of inflammation by a synthetic histone mimic. *Nature* **468,** 1119–1123
38. Lian, Z., Karpikov, A., Lian, J., Mahajan, M. C., Hartman, S., Gerstein, M., Snyder, M., and Weissman, S. M. (2008) A genomic analysis of RNA polymerase II modification and chromatin architecture related to 3′ end RNA polyadenylation. *Genome Res.* **18,** 1224–1237
39. Devaiah, B. N., Lewis, B. A., Cherman, N., Hewitt, M. C., Albrecht, B. K., Robey, P. G., Ozato, K., Sims, R. J., 3rd, and Singer, D. S. (2012) BRD4 is an atypical kinase that phosphorylates serine2 of the RNA polymerase II carboxy-terminal domain. *Proc. Natl. Acad. Sci. U.S.A.* **109,** 6927–6932
40. Barboric, M., Nissen, R. M., Kanazawa, S., Jabrane-Ferrat, N., and Peterlin, B. M. (2001) NF-κB binds P-TEFb to stimulate transcriptional elongation by RNA polymerase II. *Mol. Cell* **8,** 327–337
41. Reith, W., LeibundGut-Landmann, S., and Waldburger, J. M. (2005) Regulation of MHC class II gene expression by the class II transactivator. *Nat. Rev. Immunol.* **5,** 793–806
42. Takahashi, H., Parmely, T. J., Sato, S., Tomomori-Sato, C., Banks, C. A., Kong, S. E., Szutorisz, H., Swanson, S. K., Martin-Brown, S., Washburn, M. P., Florens, L., Seidel, C. W., Lin, C., Smith, E. R., Shilatifard, A., Conaway, R. C., and Conaway, J. W. (2011) Human mediator subunit MED26 functions as a docking site for transcription elongation factors. *Cell* **146,** 92–104
43. Heintzman, N. D., Hon, G. C., Hawkins, R. D., Kheradpour, P., Stark, A., Harp, L. F., Ye, Z., Lee, L. K., Stuart, R. K., Ching, C. W., Ching, K. A., Antosiewicz-Bourget, J. E., Liu, H., Zhang, X., Green, R. D., Lobanenkov, V. V., Stewart, R., Thomson, J. A., Crawford, G. E., Kellis, M., and Ren, B. (2009) Histone modifications at human enhancers reflect global cell-type-specific gene expression. *Nature* **459,** 108–112
44. Legube, G., and Trouche, D. (2003) Regulating histone acetyltransferases and deacetylases. *EMBO Rep.* **4,** 944–947